Skoltech

Skolkovo Institute of Science and Technology

MASTER'S THESIS

Hall effect non-linearity in two-component hybrid two-dimensional systems

Master's Educational Program: Photonics and Quantum Materials

Student: _____

Alexey Shupletsov

Research Advisor: _____

Mikhail Skvortsov
Associate Professor, CREI: Skoltech
Center for Photonics and Quantum Materials

Co-Advisor: _____

Alexander Kuntsevich
Senior Researcher, P.N.Lebedev Physical Institute of Russian Academy of Science

Moscow 2019

Skoltech

Skolkovo Institute of Science and Technology

МАГИСТЕРСКАЯ ДИССЕРТАЦИЯ

Нелинейность эффекта Холла в двухкомпонентных гибридных двумерных системах

Магистерская образовательная программа: Фотоника и квантовые материалы

Студент: _____

Алексей Шуплецов

Научный руководитель: _____

Михаил Скворцов
Доцент, Сколтеховский Центр
Фотоники и Квантовых Материалов

Со-руководитель: _____

Александр Кунцевич
Старший научный сотрудник,
Физический Институт Российской
Академии Наук им. П.Н.Лебедева

Москва 2019

Hall effect non-linearity in two-component hybrid two-dimensional systems

Alexey Shupletsov

Submitted to the Skolkovo Institute of Science and Technology
on June 18, 2019

Abstract

Laterally modulated two-dimensional systems serve as a tunable media demonstrating various effects, interesting both for fundamental physics and for potential applications. From the first principles, modulation leads to essential changes when the modulation period is less or comparable with any characteristic length of the system (mean free path, coherence length, phase coherence length etc.). At the same time, in the opposite, classical limit (modulation period is much bigger than any characteristic length of the system) the system is still heterogeneous and is expected to depend on the properties of the modulation. In this work the experimental investigation of conventional 2D system in the metal-oxide-semiconductor structure with lateral modulation in a form of an array of macroscopic islands is carried out. Besides temperature and magnetic field, the electron densities in the islands array and residual 2D gas parametrize the system (they both can be controlled independently). Thus, investigated system serve as an effective media with two subsystems and large space of parameters. The magnetotransport measurements of such system revealed different regimes of the current transport: residual 2D gas-dominated, islands-dominated, shells(the transition regions)-dominated and insulating. The regimes are characterized by different behavior of Hall coefficient with magnetic field and gate voltage, temperature dependence of resistivity and Shubnikov-de Haas patterns. The results presented in my thesis show the feasibility of this system to be used as laterally modulated two-dimensional effective media in potential applications.

Research Advisor:
Name: Mikhail Skvortsov
Degree: Doctor of Science
Title: Associate Professor, CREI: Skoltech Center for Photonics and Quantum Materials

Co-Advisor:
Name: Alexander Kuntsevich
Degree: PhD
Title: Senior Researcher, P.N.Lebedev Physical Institute of Russian Academy of Science

Acknowledgments

First of all, I want to thank people who directly participated in the work which results I describe here: Martyn Nunuparov for provided samples and Kirill Prikhod'ko for TEM measurements. I wish to express my thanks to all people who supported me during all my university education: my colleagues, mates, members of football team. I'm very grateful to my nearest colleagues Nikolai Semenov and Sergey Volosheniuk for numerous discussions and talks as about physics and our work as about life, music or Ukraine. I received very helpful input from Nikita Raginov in fabrication process - completely new part of working process for me. It was a great pleasure for me to discuss various topics with Evgeniy Gorbachev. Evgeniy also taught me some technical processes and tricks that were very helpful in my work. Also I'd like to acknowledge Maxim Litskevich - the guy whom I was starting my scientific path with. Despite the fact that he went his own way, the discussions, lessons and exams which we had together, I find at least interesting and nostalgic. Finally, the big thanks goes to Alexander Kuntsevich, my research supervisor, for his involvement in my progress and his help as by advices as by real participation. And, of course, I'd like to express my tremendous love and gratitude to my family: my warm-hearted mother, calm father and cool brother. A special thanks to my wonderful grandmothers who always were, are and will be in my life.

Contents

List of Figures

Chapter 1

Introduction

2D systems gained a lot of interest from physicists as the systems where some effects emerge or are enhanced due to lower dimensionality. Also these systems were tunable and, therefore, were very perspective for applications. After exfoliation of graphene and fabrication a sample for transport measurements out of flake performed by Geim and Novoselov in 2004[1] without sophisticated and expensive molecular beam epitaxy growth techniques (the authors won Nobel Prize 2011 for this), the interest to 2D systems increased significantly. Past years lots of systems such as two-dimensional dichalcogenides[2], topological insulators[3] etc.[4] have been reopened and actively explored. Another important feature of all 2D structures is a possibility of easy control of their properties by changing the density of charge carriers through gate voltage. Nowadays the physics of 2D systems has become essential and rapidly developing part of condensed matter physics and such systems serve convenient platforms for numerous physical experiments and applications.

The lateral modulation of 2D systems opens extra functionality and can lead to new interesting effects such as gate-tunable superconductivity in a lattice of superconducting tin islands on graphene[5], recent discovery of correlated state and superconductivity in magic-angle twisted bilayer graphene [6, 7], experimental observation of Holfstatder's butterfly[8], commensurability effects in semiconducting quantum wells with lateral modulation[9], selectivity to circularly polarized light in chiral laterally modulated structures[10] etc. Modulation period is typically much less than any characteristic length of the system (mean free path, coherence length, phase coherence length for example) and the related effects weaken with the increase of modulation length. On the other hand, even in opposite limit, when modulation period is much bigger than effective length, the system still remains heterogeneous and serve as effective media. This limit wasn't explored yet, so it was decided to investigate 2D system with macroscopic modulation in the form of array of areas (which are called islands further) that are controlled by separate gate.

In this thesis the examination of the conductive properties of laterally modulated 2D system that is based on archetypal Si-MOSFET platform is demonstrated through magnetotransport measurements. Such system is similar to granular materials, studied broadly in the past[11] but differs from them by: (i) complete two-dimensionality and tunability of both parent electron gas and islands; (ii) periodicity, i.e. absence of randomness in positions of islands; (iii) smooth transition

regions (larger than mean free path) between parent gas and islands.

Previously the transport studies of modulated semiconducting 2D systems were focused either on clean systems (where mean free path is larger than the period of modulation and all studied phenomena are essentially ballistic[12, 13, 14, 15, 16]) or on Aharonov-Bohm/Altshuler-Aharonov-Spivak oscillations[17, 18], i.e. coherent low-temperature mesoscopic effects[19, 20, 21]. All these phenomena are essentially nano-scale. I should also mention a group of a papers[22, 23, 24, 25, 26], where percolation and transition to localization phenomena in the arrays of dots/anti-dots were explored. Thus, the analysis of the effects in macroscopically modulated 2D system in diffusive regime of current flow performed in this work is scientifically valid.

Chapter 2

Theoretical basics

2.1 MOSFETs and 2D systems

The textbook example of 2D system is Metal-Dielectric-Semiconductor(MDS) structures. The most common structures of this type are the ones produced on the basis of silicon with SiO_2 oxide as dielectric which, therefore, are called silicon Metal-Oxide-Semiconductor(MOS) structures. Such structures let people obtain 2D system on the interface between Si and SiO_2 with controlled electron (hole) density through voltage to metal, which is called gate. On the fig.2.1 shown the schematic image of MOS Field-Effect-Transistor(FET) which is very broadly used in industry as an element of logic schemes in modern microelectronics due to its feature to be opened (conductive regime) or closed (isolating regime) depending on controlled parameter - gate voltage.

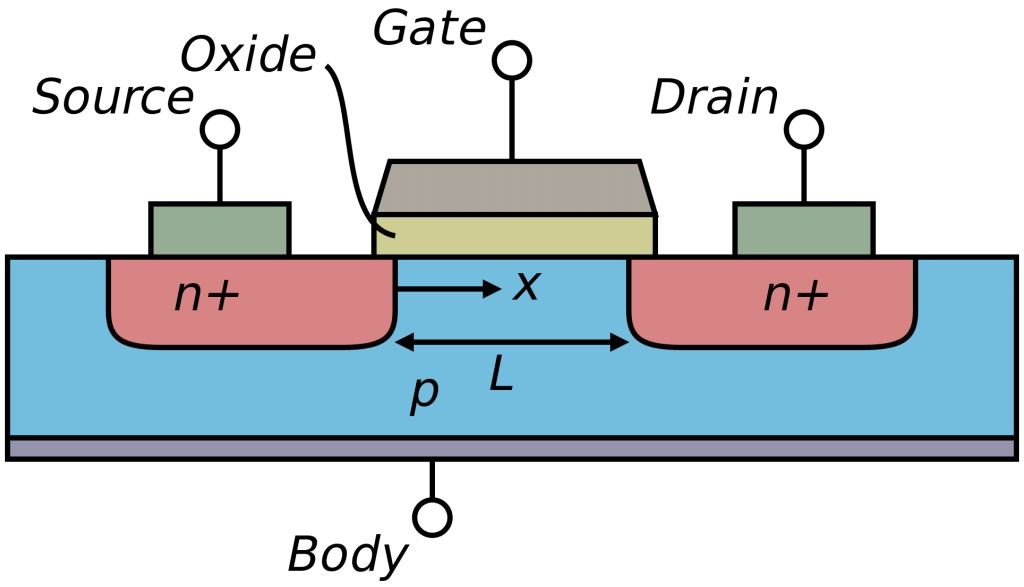

Figure 2.1: The scheme of MOSFET. p means weakly doped p-type semiconductor, whereas $n+$ means highly doped n-type semiconductor

Two-dimensionality means that the electron motion is possible only in two directions. In terms of quantum mechanics it means that wave function of charge carrier is localized along one axis. In other words, the effect of dimensional quantization occurs, i.e. the size of classically al-

lowed region (where potential energy less than energy of carrier) becomes comparable with wavelength of the carrier. It leads to quantization of momentum along this axis, so only two components of momentum leave free.

As well-known from university course of solid state physics(SSP), Bloch theorem restricts the possible values of electron wave numbers inside crystals that leads to the emergence of prohibited areas of carriers energy, i.e. the formation of energy bands (it is called band structure)[27]. From common principles carriers fill low-energy states until some level that is called Fermi energy. For further terminology: the nearest to Fermi level zone with higher energies is called conduction band, whereas nearest zone with lower energies - valence band. Also there is difference between real electrons that round around nucleus and so-called quasiparticles that serve as charge carriers in crystals. Quasiparticles have such name as they are just objects that are convenient for theoretical description of processes in crystals, this is not real particles. The quasiparticles that emerge in conduction band are also called electrons whereas emerged in valence band are called holes. Fermi level lies deeply under the level of carrier energy in vacuum that means the crystal is stable. The difference between the energy of carrier in vacuum and Fermi energy is called work function. For simplicity, further we assume that work functions of metal and semiconductor are equal. The metal in SSP means that Fermi level lies inside some band, in insulator Fermi level lies inside he gap and the gap is relatively big. Semiconductor is intermediate state: Fermi level lies inside the gap, but gap is quite small and, for example, temperature can induce charge carriers in bands. We consider p-type semiconductor that means that semiconductor is doped with acceptor atoms, i.e. those who have less valence electrons than parent atoms (the atoms that have more valence electrons are called donors). In terms of band structure it means that Fermi energy lies near or slightly in valence band. Semiconductor and metal are electrically tied through DC voltage source such that semiconductor potential is taken as zero and metal potential is counted in positive direction. Move further and look how the application of gate voltage changes MOSFET structure.

This problem can be solved exactly[28] by applying Boltzmann distribution of electrons and holes:

$$n_p = n_{p0} \cdot exp(e\varphi/kT) \tag{2.1}$$

$$p_p = p_{p0} \cdot exp(-e\varphi/kT) \tag{2.2}$$

where e - elementary charge ($e > 0$), T - temperature, k - Boltzmann constant, φ - electrical potential, n_{p0} and p_{p0} - equilibrium (deep inside the crystal where potential is zero) electrons and holes density, respectively

and 1D Poisson equation:

$$\frac{d^2\varphi}{dx^2} = -4\pi\frac{\rho(x)}{\epsilon} \tag{2.3}$$

where ϵ - permittivity of semiconductor, $\rho(x)$ - volume charge density:

$$\rho(x) = e(N_D^+ - N_A^- + p_p - n_p) \tag{2.4}$$

where N_D^+ and N_A^- - density of ionized donor and acceptor atoms, respectively.

Moreover, deep inside semiconductor, where $\varphi = 0$, electroneutrality condition is met, i.e. $\rho(x) = 0$, therefore

$$N_D^+ - N_A^- = n_{p0} - p_{p0} \tag{2.5}$$

These relations are enough to solve the problem and obtain the dependencies of the electrical potential, field and density of charge carriers on coordinate. As the final expressions are very bulky and complex, here I will give a qualitative description only. It can be obtained by applying energetic diagrams pictures - the schematic dependence of charge carriers full energy from coordinate. Inside the semiconductor the levels must remain unchanged, whereas in the metal all levels must be shifted by eV value above. Conductivity of bulk metal is much better than conductivity of bulk semiconductor that let us consider metal as equipotential volume. Than on the interface between the semiconductor and the oxide (as inside oxide) the distortion of energy levels occur.

Considering all simplifications, at zero gate voltage $V_g = 0$ energy diagram is shown in Fig.2.2a. Further discussion is based on equilibrium condition: electrochemical potential $\phi = \varepsilon_F - e\varphi$ must be equal along the whole system. Therefore by applying negative voltage to metal the Fermi level in metal raises on the value $-eV$. In semiconductor the potential decreases and, therefore, the valence band edge curls up. It is illustrated on the fig.2.2b.

More interesting case is applying positive voltage $V_g > 0$. Then the Fermi level in metal lowers as well as edges of bands in semiconductor (fig.2.2c). By applying relatively high V_g the edge of conduction band ε_c intersect electrochemical potential and states below electrochemical potential on the interface between semiconductor and oxide emerge. At zero temperature all states below ϕ are filled and all states above are empty. Thus, on the interface between semiconductor and oxide quite narrow layer of classically allowed states emerges that is called inversion layer. It has such name because in p-type semiconductor, where main carriers in bulk are holes, the layer of electrons emerges. Moreover, it is worth to mention that behind the inversion layer (farther from oxide) the depletion region emerges - the region where the electrochemical potential lies relatively far as from the bottom of conduction band ε_c as from the top of the valence band ε_v. Therefore in this region at low temperatures there are no charge carriers.

It is important to obtain the dependence of electron density from gate voltage. Considering only conductive regime of MOSFET (when the inversion layer exists) almost all charge in semiconductor is collected in the inversion layer. System is electrically neutral as the whole, therefore the charge in the metal must compensate the charge in semiconductor. Metal always collect charge on

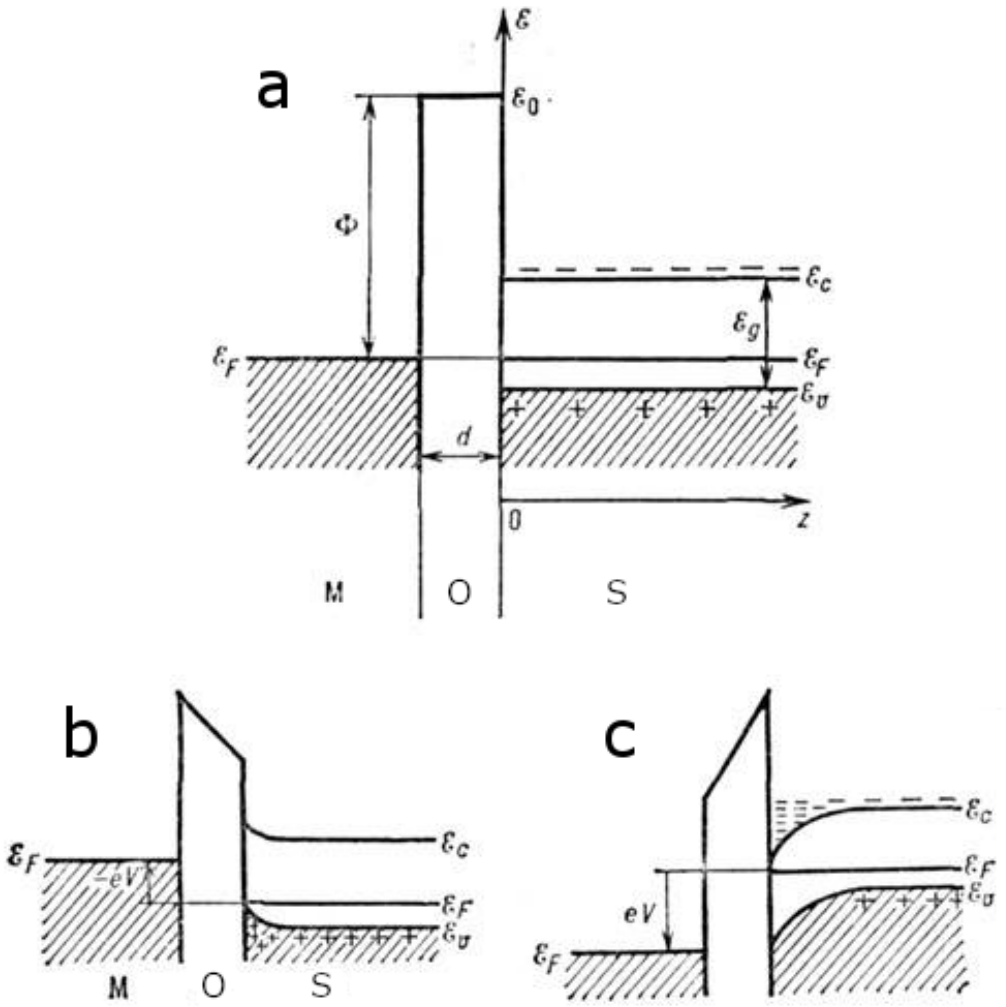

Figure 2.2: Energetic (band) diagrams of MOS transition: (a) at zero gate voltage $V_G = 0$, (b) at $V_G < 0$, (c) at $V_G > 0$ [28]

the boundary, therefore the effective capacitor emerges: negative plate is inversion layer, positive plate is the boundary of metal, the surface density is n, applied voltage is V_g. At this moment take into account that semiconductor and metal have different work functions. It just means that it is needed to apply some threshold voltage V_{th} to compensate this difference and reduce the problem to considered one (when the band edges were straight at V_g=0). Following Gauss relation it can be written:

$$E = \frac{4\pi en}{\epsilon} \tag{2.6}$$

where ϵ - silicon oxide SiO_2 permittivity.

Also oxide can store some randomly distributed charges that are frozen in dielectric. It also leads to some additional potential difference needed to make band edges straight. Thus, the total gate voltage is summed up from V_{th} originating from work functions difference and stored charge

in dielectric and from V_c produced by surface charges and falling on the dielectric:

$$V_g = V_{th} + \frac{4\pi en}{\epsilon} d \tag{2.7}$$

where d - oxide thickness.

To sum up, $n \propto \frac{V_g - V_{th}}{d}$, where V_g - gate voltage, V_{th} - threshold voltage, d - oxide thickness.

2.2 2D systems behavior in weak magnetic fields

Let's consider how 2D system behaves itself being subjected to magnetic field in direction perpendicular to the plane of the system. Kinetic Boltzmann equation:

$$\frac{\partial f}{\partial t} + \vec{v}\frac{\partial f}{\partial \vec{r}} + \vec{F}\frac{\partial f}{\partial \vec{p}} = St[f] \tag{2.8}$$

where f - electron distribution function, $St[f]$ - collision integral

As we are considering stationary and homogeneous problem, the first and the second term vanish. Electrons are subjected to electrical $\vec{E}$ and magnetic $\vec{B}$ fields, therefore:

$$\vec{F} = -e\vec{E} - \frac{e}{c}\left[\vec{v} \times \vec{B}\right] \tag{2.9}$$

Minuses comes from negative charge of the electron (taking $e > 0$). Here is tau-approximation for Boltzmann equation:

$$St[f] = -\frac{\delta f}{\tau} \tag{2.10}$$

where $\delta f = f - f_0$, f_0 - equilibrium distribution function

Also notice, that $\frac{\partial f_0}{\partial \vec{p}} = \frac{\partial f_0}{\partial \varepsilon}\frac{\partial \varepsilon}{\partial \vec{p}} = \vec{v}\frac{\partial f_0}{\partial \varepsilon}$. In term with electric field change f derivative with f_0 derivative because we suppose $\delta f \ll f_0$. The same can't be performed with the term with magnetic field because force applied to electron from magnetic field is perpendicular to electron velocity, therefore scalar multiplication this force and electron velocity is equal to 0. That's why we have:

$$e\tau\left(\vec{v}\cdot\vec{E}\frac{\partial f_0}{\partial \varepsilon} + \frac{\left[\vec{v}\times\vec{B}\right]}{c}\frac{\partial \delta f}{\partial \vec{p}}\right) = \delta f \tag{2.11}$$

From this point all subsequent reasoning are made for 2D systems with parabolic expression for energy dispersion. For such systems the momentum and velocity of charge carrier are directly proportional to each other and the coefficient of proportionality is equal to effective mass of the carriers. Let's find δf in the following form: $\delta f = \vec{p}\cdot\vec{\chi}$. Then the derivative $\frac{\partial \delta f}{\partial \vec{p}}$ can be changed on $\vec{\chi}$ as the second term is proportional to $\vec{p}$, therefore it will be shrunk after scalar multiplication

with the force from magnetic field. Besides it is worth to mention that $\left[\vec{v}\times\vec{B}\right]\cdot\vec{\chi}=\left[\vec{B}\times\vec{\chi}\right]\cdot\vec{v}$. As $\vec{v}$ can have arbitrary direction, the vectors, that are multiplied by $\vec{v}$ from the left and right sides of equation sign, have to be equal:

$$\vec{\chi}=\frac{e\tau}{m}\left(\frac{\partial f_0}{\partial\varepsilon}\vec{E}+\frac{1}{c}\left[\vec{B}\times\vec{\chi}\right]\right) \tag{2.12}$$

Let's make, firstly, scalar and, secondly, vector multiplications of both sides of the equation by $\vec{B}$. Using equation $\vec{B}\times\left[\vec{B}\times\vec{\chi}\right]=\left(\vec{B}\vec{\chi}\right)\vec{B}-B^2\vec{\chi}$ obtain three equations (with the primordial one):

$$\vec{B}\cdot\vec{\chi}=\frac{e\tau}{m}\frac{\partial f_0}{\partial\varepsilon}\vec{B}\cdot\vec{E} \tag{2.13}$$

$$\left[\vec{B}\times\vec{\chi}\right]=\frac{e\tau}{m}\left(\frac{\partial f_0}{\partial\varepsilon}\left[\vec{B}\times\vec{E}\right]+\frac{1}{c}\left(\vec{B}\vec{\chi}\right)\vec{B}-\frac{B^2}{c}\vec{\chi}\right) \tag{2.14}$$

$$\vec{\chi}=\frac{e\tau}{m}\left(\frac{\partial f_0}{\partial\varepsilon}\vec{E}+\frac{1}{c}\left[\vec{B}\times\vec{\chi}\right]\right) \tag{2.15}$$

Using expression for $\vec{B}\cdot\vec{\chi}$ from the first equation in the second one and then $\left[\vec{B}\times\vec{\chi}\right]$ from the second to the third one. Then getting expression for $\vec{\chi}$:

$$\vec{\chi}=\frac{c}{1+\left(\frac{e\tau}{mc}\right)^2\cdot B^2}\frac{\partial f_0}{\partial\varepsilon}\cdot\left(\frac{e\tau}{mc}\vec{E}+\left(\frac{e\tau}{mc}\right)^2\left[\vec{B}\times\vec{E}\right]+\left(\frac{e\tau}{mc}\right)^3\left(\vec{B}\vec{E}\right)\vec{B}\right) \tag{2.16}$$

Expressions for electron density and current density through distribution function:

$$n=\int f d\Gamma_{\vec{p}}\equiv\int f_0 d\Gamma_{\vec{p}} \tag{2.17}$$

$$\vec{j}=-e\int f\vec{v}d\Gamma_{\vec{p}}\equiv-e\int\delta f\vec{v}d\Gamma_{\vec{p}} \tag{2.18}$$

If integrand depends only on the energy, then $d\Gamma_{\vec{p}}$ can be changed onto $D(\varepsilon)d\varepsilon$, where $D(\varepsilon)=\frac{dN}{d\varepsilon}$ - density of states. Applying easily calculations, it can be obtained:

$$D(\varepsilon)\ \propto\ \begin{cases}\frac{1}{\sqrt{\varepsilon}} & \text{if } d=1\\ const & \text{if } d=2\text{, where } d\text{ - dimensionality}\\ \sqrt{\varepsilon} & \text{if } d=3\end{cases} \tag{2.19}$$

From the course of field theory it is known that $\int\left(\vec{p}\vec{A}\right)\vec{p}d\Omega_{\vec{p}}=\frac{\vec{A}}{d}\cdot\int p^2 d\Omega_{\vec{p}}$, where $\vec{A}$ - constant vector, d - dimensionality, $d\Omega_{\vec{p}}$ - an element of solid angle in the space of vector $\vec{p}$.

Considering that τ doesn't depend on energy and taking into account that $\vec{p}\cdot\vec{v}=2\varepsilon$ the

expression for current density becomes:

$$\vec{j} = \frac{2}{d}\frac{ec}{1+\left(\frac{e\tau}{mc}\right)^2 \cdot B^2}\left(\frac{e\tau}{mc}\vec{E} + \left(\frac{e\tau}{mc}\right)^2\left[\vec{B}\times\vec{E}\right] + \left(\frac{e\tau}{mc}\right)^3\left(\vec{B}\vec{E}\right)\vec{B}\right)\cdot \\ \cdot\int\left(-\frac{\partial f_0}{\partial\varepsilon}\right)\varepsilon D(\varepsilon)d\varepsilon \tag{2.20}$$

Applying $D(\varepsilon)$ dependence the following dependence is right: $\varepsilon D(\varepsilon) \propto (\varepsilon)^{\frac{d}{2}}$. Then integral in expression for $\vec{j}$ can be integrated by parts. Free term is zero as $f_0 = \frac{1}{exp\left(\frac{\varepsilon-\mu}{T}\right)+1}$ - Fermi distribution. Then, taking into account an expression for n, the following formula is obtained:

$$\vec{j} = \frac{ne^2\tau}{m}\frac{1}{1+\left(\frac{e\tau}{mc}\right)^2 \cdot B^2}\left(\vec{E} + \frac{e\tau}{mc}\left[\vec{B}\times\vec{E}\right] + \left(\frac{e\tau}{mc}\right)^3\left(\vec{B}\vec{E}\right)\vec{B}\right) \tag{2.21}$$

This is an expression in CGS system. In SI the expression for force from the magnetic field to electron doesn't include c. That's why in SI in expression for $\vec{j}$ all c are absent. Since for the description of the systems the concept of carriers mobility is used, find the expression for μ via τ and m. Carriers mobility is the coefficient between absolute value of drift velocity and absolute value of of applied electrical field in absence of magnetic field: $|\vec{v}| = \mu\left|\vec{E}\right|$. Drift velocity is an average speed of electron, the speed of electron stream. Since $\vec{j} = ne\vec{v}$, where $\vec{v}$ - drift velocity, applying expression 2.21 for $\vec{j}$, in zero magnetic field $\vec{j} = \frac{ne^2\tau}{m}\vec{E}$, that leads to the following expression for electron mobility μ:

$$\mu = \frac{e\tau}{m} \tag{2.22}$$

Conductivity tensor $\sigma_{\alpha\beta}$ is introduced by definition as $j_\alpha = \sigma_{\alpha\beta}E_\beta$. Resistivity tensor is reciprocal to the conductivity tensor $\rho_{\alpha\beta} = (\sigma_{\alpha\beta})^{-1}$. Choosing Z direction along vector of magnetic field $\vec{B}$ from expression for $\vec{j}$ written above the following formulas for tensors are obtained:

$$\sigma_{\alpha\beta} = \frac{\sigma_0}{1+(\mu B)^2}\begin{pmatrix} 1 & -\mu B & 0 \\ \mu B & 1 & 0 \\ 0 & 0 & 1+(\mu B)^2 \end{pmatrix} \tag{2.23}$$

$$\rho_{\alpha\beta} = \begin{pmatrix} \sigma_0^{-1} & RB & 0 \\ -RB & \sigma_0^{-1} & 0 \\ 0 & 0 & \sigma_0^{-1} \end{pmatrix} \tag{2.24}$$

where

$$\begin{aligned} \mu &= \frac{e\tau}{m} \text{ - electron mobility} \\ \sigma_0 &= \frac{ne^2\tau}{m} \text{ - Drude conductivity} \\ R &= \frac{1}{ne} \text{ - Hall coefficient} \end{aligned} \tag{2.25}$$

Here are the expressions that have been obtained here and are important for following narration:

$$\begin{aligned} \sigma_{xx} &= \frac{\rho_{xx}}{\rho_{xx}^2 + \rho_{xy}^2} \\ R &= \frac{\rho_{xy}}{B} = \frac{1}{ne} \\ \rho_{xx} &= \frac{m}{ne^2\tau} = \frac{1}{ne\mu} \end{aligned} \tag{2.26}$$

Obtained results allow to determine the most important parameters of electron gas such as concentration n and mobility μ from magnetotransport measurements. Firstly, that is seen from expression for resistivity tensor $\rho_{\alpha\beta}$, longitudinal term is symmetric in terms of magnetic field, whereas transverse is antisymmetric. As an asymmetry of contacts is always present, data with mixed components of tensor is always obtained out of the experiment. The components are easily separated by symmetrization (for ρ_{xx}) and antisymmetrization (for ρ_{xy}) of measured values in terms of field. Secondly, for determination of electron density of 2D gas it's enough to measure ρ_{xy} at $B = \pm 1T$ and take the half of their difference (antisymmetrization). Obtained value is Hall coefficient, that reciprocal to electron density and equal to $625\frac{\text{Ohm}}{T}$ at $n = 10^{-12}\text{cm}^{-2}$. Finally, mobility is equal to the Hall coefficient relation to the half of the sum ρ_{xx} in symmetrical weak fields ($B = \pm 1T$, for example). At higher fields the oscillations of resistivity start whereas sharp maximum is observed at values close to zero. It is connected with weak localization and has purely quantum nature.

2.3 2D systems behavior in strong magnetic fields

In strong magnetic fields τ-approximation is not valid anymore. It's well-known that electron spectrum in the direction perpendicular to magnetic field turns into the spectrum of quantum oscillator forming equidistant ladder of energy levels called Landau levels (LLs)[30]. For 2D systems in magnetic field perpendicular to the plane of 2D gas, the electron spectrum has the following form

(in CGS):

$$
\begin{aligned}
E_n =& \hbar\omega_c \left(n + \frac{1}{2}\right) \pm \mu_B H, \text{ where} \\
& n \in \{0, 1, 2...\} \\
& H \text{ - magnetic field} \\
& \mu_B = \frac{\hbar e}{2 m_e c} \text{ - Bohr magneton} \\
& \omega_c = \frac{eH}{m^* c} \text{ - cyclotron frequency}
\end{aligned}
\tag{2.27}
$$

The number of states on one Landau level per area (the degeneracy) is equal to:

$$N_L = \frac{eH}{hc} \tag{2.28}$$

From the formula 2.27 it is seen that Bohr magneton is expressed through free electron mass m_e, whereas cyclotron frequency - through effective mass m^*. The latter usually much smaller than m_e, therefore Zeeman splitting (the second term in expression for E_n), that emerges due to the presence of spin from electron, is usually neglected. Moreover, in the formula 2.27 the g-factor was taken to be 2 as for free electrons, while in crystal g-factor can differ from 2. For ideal crystal the dependence of density of states on energy has a form shown in Fig.2.3a - a set of delta-functions at $\varepsilon = \hbar\omega_c \left(n + \frac{1}{2}\right)$. However the presence of disorder leads to broadening of Landau levels (shown in Fig.2.3b).

Electrons are fermions therefore their distribution function has the following form (Fermi-

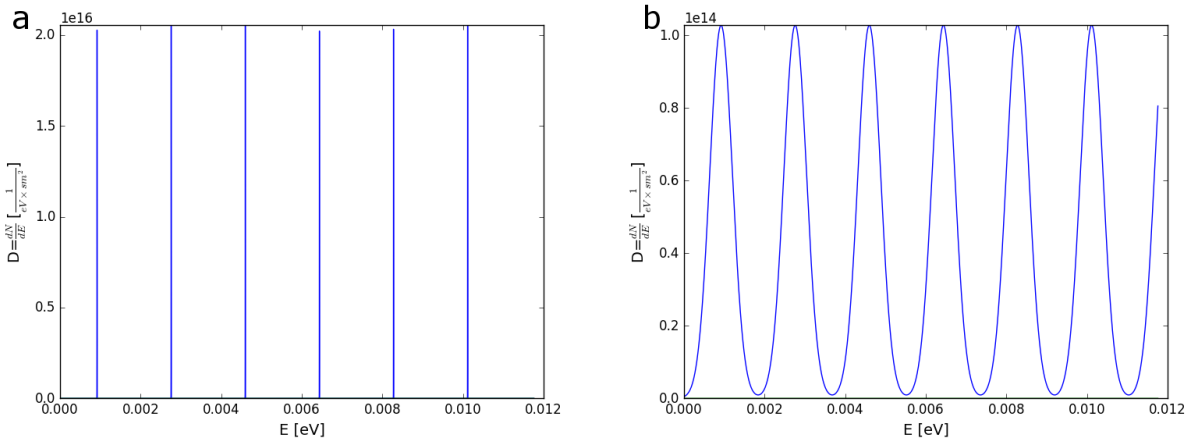

Figure 2.3: Dependence of density of states of 2D electron gas in crystal in magnetic field: (a) ideal crystal; (b) crystal with disorder

Dirac function):

$$f_0 = \frac{1}{exp\left(\frac{\varepsilon - \mu}{T}\right) + 1} \tag{2.29}$$

At zero temperature all states below the Fermi level μ are filled and all states above are empty. At nonzero temperature the precise border between filled and empty states is blurred near the Fermi level on the value of order T. Therefore the derivative $\frac{\partial f_0}{\partial \varepsilon}$ has a form of narrow peak near the Fermi level. On the order of temperature (i.e. width of this peak) the density of states usually is a smooth function, therefore in the integral of the expression $\frac{\partial f_0}{\partial \varepsilon} D(\varepsilon)$ over energy density of states can be taken constant and equal to the value at Fermi level and be taken away from the integral.

From expression 2.16 δf is proportional to $\frac{\partial f_0}{\partial \varepsilon}$. This δf is placed under integral over $d\Gamma_{\vec{p}} = D(\varepsilon)d\varepsilon$ in expression for current $\vec{j}$. From everything mentioned above the following dependence comes out:

$$\sigma_{xx} \propto D(\mu) \tag{2.30}$$

With the growth of magnetic field, the degeneracy of LL N_L increases as well as cyclotron frequency. As Fermi level is defined as energy level under which the number of states is equal to electron density in the system, the magnetic field-dependence of the Fermi level has a shape of zigzag. Considering the position of Fermi level relatively to LLs at more realistic picture of blurred LLs, the Fermi level moves to left (smaller number of LL). Therefore, with increase of magnetic field the longitudinal conductivity σ_{xx} increases until Fermi level reaches the peak of LL and then starts to decrease. Thus, σ_{xx} has clear maximums at values defined from condition $\mu = \hbar\omega_c \left(N + \frac{1}{2}\right)$. As LL are symmetrical, when Fermi level is placed in the center of N level, the half of this level is filled. So, N levels are filled (the counting starts from zero) and (N+1) level is half-filled:

$$\begin{aligned} n =& \nu N_L \left(N + \frac{1}{2}\right), \text{ where} \\ & \nu \text{ - degeneracy rate (valley and spin)} \\ & n \text{ - electron density} \end{aligned} \tag{2.31}$$

Often in 2D systems electron density is fixed (i.e. by gate voltage), so $n = const$. Then the following expression is obtained:

$$N = \alpha + \beta\frac{1}{H}, \text{ where } \alpha, \beta = const \tag{2.32}$$

So the dependence of maximum number on inverse values of field is a straight with slope:

$$\beta = \frac{hc}{e\nu}n \tag{2.33}$$

This expression let measuring the electron density from resistivity oscillations. As the same reasoning could be made for minimum (then $\mu = \hbar\omega_c N$ and the integer number of LLs $n = \nu N_L N$

is filled), it is not important if the straight is built out of minimum or maximum positions: the dependence of number of maximum (minimum) has to be built from reverse values of magnetic field at which this maximum (minimum) occurs. Then the straight line should be built interpolating the dots, the slope of this line is determined and from formula

$$n = \nu \frac{e\beta}{hc} \tag{2.34}$$

electron density can be found. For silicon ν=4 as electrons has two-fold degeneracy from spin and silicon has two equivalent valleys. Such oscillations are called Shubnikov-de Haas oscillations (SdHO). The formulas above are written in CGS.

As it was mentioned, Zeeman splitting is quite small relative to cyclotron frequency (the distance between LLs) but it is present. Its influence reduces to the formation of two closely positioned "humps" out of one peak. At relatively big magnetic field the Zeeman splitting is big enough that σ_{xx} reaches first "hump", decreases a little bit, then again starts to increase and reaches another "hump". Thus, the splitting of the longitudinal conductivity σ_{xx} maximum occurs when Zeeman splitting is significant.

2.4 Metal-insulator transition in 2D systems

Ultimate behavior of the resistivity in the $T \to 0$ limit has always been one of the major problems in the solid state physics. This question has quite rich story[31]. All systems are divided in two groups on the basis of temperature dependence of resistivity - metals and insulators. For typical metals at T=0K a presence of finite value of resistivity $\rho = \rho_{imp}$, where ρ_{imp} comes from electron scattering onto impurities, is typical. With temperature increasing the metal resistivity also increases, therefore if the system has positive temperature the derivative of the resistivity $\frac{d\rho}{dT} > 0$ it is called the *metallic* state of the system. Insulators are very diverse but all of them are characterized by spatial localisation of electron that obstructs the conductivity of current. Therefore the insulators are characterized by infinite growth of resistivity at zero-temperature limit. If the system has negative temperature derivative of resistivity $\frac{d\rho}{dT} < 0$, it is called the *insulating* state of the system.

As it was mentioned, 2D homogeneous systems are characterized by two parameters: density n and mobility μ. The latter is directly connected with disorder in the system: the stronger the disorder, the smaller mean free path, the smaller charge carriers mobility. Besides, the cleaner the sample, the smaller densities can be obtained in it. The density bottom borderline is defined by the transition of the sample to the insulating state, where sample doesn't carry current and, therefore, magnetotransport measurements can't be proceeded.

Almost 40 years ago it was considered that 2D systems can't be in metallic state. For non-interacting systems it was proposed the scaling theory[32] that declared that at zero temperature all charge carriers become localized and the resistivity goes to infinity either logarithmically ("weak localization") or exponentially ("strong localization") with temperature decrease. Then it was determined[33] that the accounting of weak interparticle interactions leads to stronger localization. In the limits of strong interactions between electrons it was proposed the formation of Wigner crystal[34] that freezes if any disorder is present (and the disorder is always present) and doesn't carry current. The experiments were agreed with theory propositions.

It is worth to mention that electron interaction depends on electron gas density. Charged particles interacts by Coulomb law:

$$E_{\text{int}} \sim \frac{e^2}{\epsilon r} \sim \frac{e^2}{\epsilon} n^{\frac{1}{2}} \propto n^{\frac{1}{2}} \tag{2.35}$$

Whereas kinetic energy of the particles has an order of Fermi energy:

$$\begin{gathered} E_F = \frac{p_F^2}{2m^*} = \frac{4\pi\hbar^2 n}{2m^*\nu} \propto n, \text{ where} \\ \nu \text{ - degeneration (valley, spin)} \end{gathered} \tag{2.36}$$

The system is regarded as strongly interacting if interaction energy exceeds average kinetic energy and vice verse. In 2D systems the counterintuitive result is correct: the higher the density of the system, the weaker interactions inside it.

The technology of 2D structures fabrication was developed, so cleaner samples were produced where lower densities could be obtained. Some papers[35, 36, 37] appeared where metallic state of 2D systems was observed. As a result, it turned out that in 2D systems with low density and weak disorder metal-isolator transition is observed (shown in Fig.2.4). At very low densities the system behave as isolator but there is some density n_c exists such that for $n > n_c$ the system behaves as isolator for temperatures higher than T^* but has metallic behavior below this temperature. For silicon structures the following expression were proposed phenomenologically for description of resistivity behavior ρ in metallic state:

$$\rho(T) = \rho_1 + \rho_2 exp\left[-\left(\frac{T_0}{T}\right)^{\gamma}\right] \tag{2.37}$$

where ρ_1, ρ_2 and T_0 don't depend on temperature, but depend on n, relation $\frac{\rho_2}{\rho_1}$ (rate of "metallicity") decreases with growth of density, γ - constant of order 1.

Thus, 2D systems are in insulating state for any densities for the systems with strong disorder (low mobility charge carriers). If 2D systems are clean enough (carriers have high mobility $\mu \gtrsim 1\text{m}^2/\text{Vs}$) then at very low densities they are still insulators. But critical density n_c emerge so

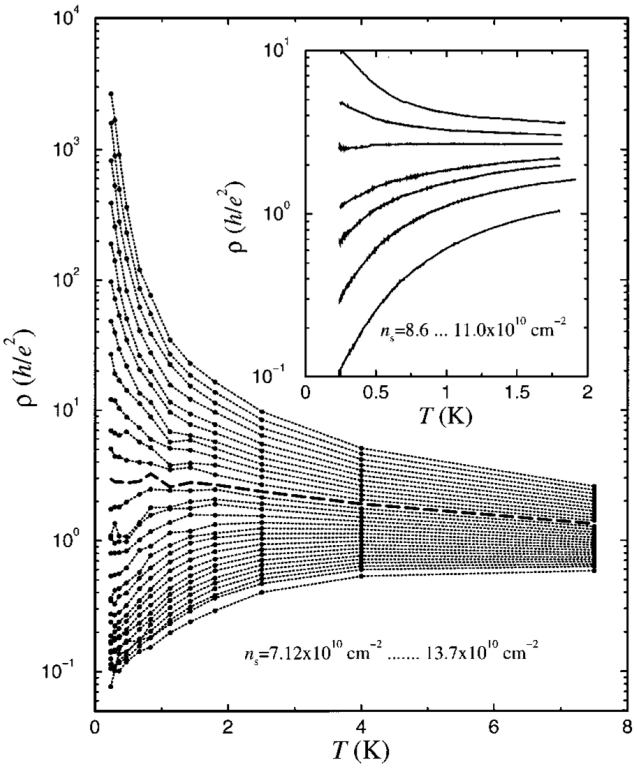

Figure 2.4: Temperature dependence of resistivity in silicon MOSFET with small densities and weak disorder for 30 different electron densities. On the insets the dependencies of resistivity on temperature near the transition from metallic to insulating behavior are shown for another sample for 7 densities (from paper [31])

that for densities above it the system demonstrates metallic behavior the stronger the closer density to the critical one. At higher densities again weak insulating behavior can be observed. It is valid for Si-based 2DES: a valuable metallicity (2-5 times growth of the resistivity from $\sim$ 1K to $\sim$ 10K) emerges only if the peak mobility is rather large ($\mu > 1$ m^2/Vs) whereas for relatively big densities weak insulating behavior is observed again.

Chapter 3

Samples and methods

3.1 Samples

In this work Si-MOSFETs structures with lithographically defined antidots array (AA) (further sometimes islands are called antidots though they can be dots) were used. The samples were produced on factory Micron in Zelenograd and provided by Martyn Nunuparov from A.M.Prokhorov Institute of General Physics of Russian Academy of Science. The optical images, TEM images with cross-section and gate connection are shown schematically on fig.3.1. Panels **a**, **b** show optical images of the sample. Diameter of the islands is 2.5 μm, lateral period d of the structure is 5 μm so that transport between them is diffusive ($l \ll d$ where $l \sim 50$ nm is mean free path in the highest mobility samples) and possible coherent effects are negligible ($l_\phi < d$ where $l_\phi < 500$nm is phase coherence length in studied temperature range). The AA has a Hall-bar shape with lateral dimensions 0.4 mm x 0.4 mm.

The structure of sample is following (the description refers to panels **c** and **d**): bottom layer in light-gray color is single crystalline (001) Si substrate; the dark color corresponds to SiO_2, areas above SiO_2 inhomogeneously colored in gray correspond to polycrystalline heavily doped Si (Si++) that, in fact, acts as metal. Trapezoidal-shaped Si++ is the gate of the antidots, the rest polycrystalline heavily doped Si is the S2DG gate. For in-plane structure the following picture can be helpful: conventional MOSFET with Si++ on the top was taken and applying lithography technique the array of holes till the oxide was etched. Then the whole sample was burned for forming silicon oxide on the top, i.e. the holes rested the same (there already SiO_2 was on the top), whereas the gate (Si++) became buried under layer of oxide. Then just another layer of Si++ on the top was created. This layer is gate for islands as in area out of islands the potential of this gate is screened by S2DEG gate, lying beneath.

Panel **d** shows the zoom in of the edge of the island. It is clearly seen that the oxide layer becomes thicker closer to the edge of the S2DG. This leads to lower density of electrons in the domains underneath. Moreover, gate electrodes are separated by oxide so that between antidots and S2DG there is a region where density is expected to be low. We call these transition regions *shells*. The panel **e** shows the same spot as panel **b** with all mentioned above areas in color.

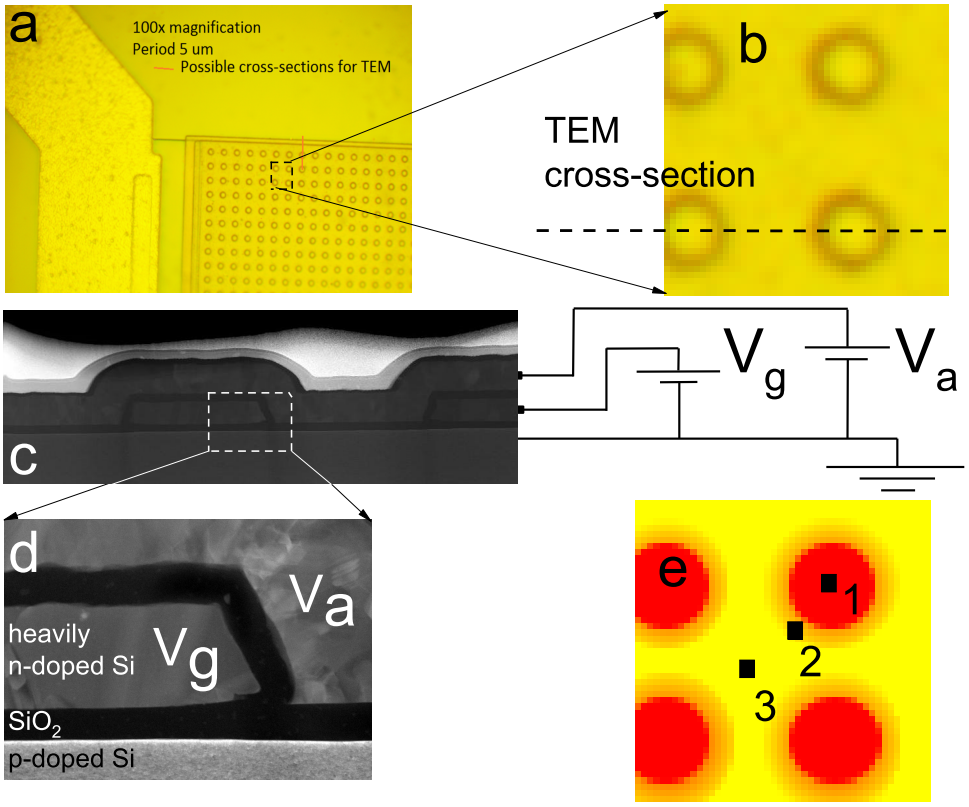

Figure 3.1: (a) Optic image of the corner of the AA (100x magnification), (b) zoom-in of image (a) with direction of slice for TEM, (c) TEM image with scheme of the gating, (d) TEM image of the border of the island (on the right), S2DG (on the left) and shell (between), (e) image (b) with signed areas (1-island, 2-shell, 3-SD2G).

The system has 7 contacts pads: source (S), drain (D), potential contacts (V_{xx}, V_{xy}, V_{xxxy}) and two gate contacts (G_a and G_g). The whole optical image of investigated sample with signed contact pads is shown on fig.3.2.

Contacts S and D are called current contacts. They are connected to heavily doped with donors areas in weakly doped with acceptors silicon substrate (schematically shown on fig.2.1). The inversion layer (investigated 2D system) is formed on the interface between substrate and oxide in vertical direction and between these areas in plane. It is important that the contact between $S(D)$ and AA is made across the whole sides of inversion layer as current injection occurs evenly across the side of AA and, therefore, it is not needed to reason about heterogeneous spreading of current and effects connected with it.

Gate contacts G_a and G_g are connected to corresponding layers of polycrystalline silicon. Voltages are applied to these electrically decoupled gate electrodes that independently control the density of the electrons (i) inside the islands (V_a) and (ii) in the surrounding 2D gas (S2DG) (V_g). As it was discussed earlier, some voltage on G_g is needed just to form 2D system.

Potential pads are just connected to the inversion layer at some points: V_{xx} and V_{xxxy} on the same side, V_{xxxy} and V_{xy} opposite to each other. Unlike the current contacts, potential contacts

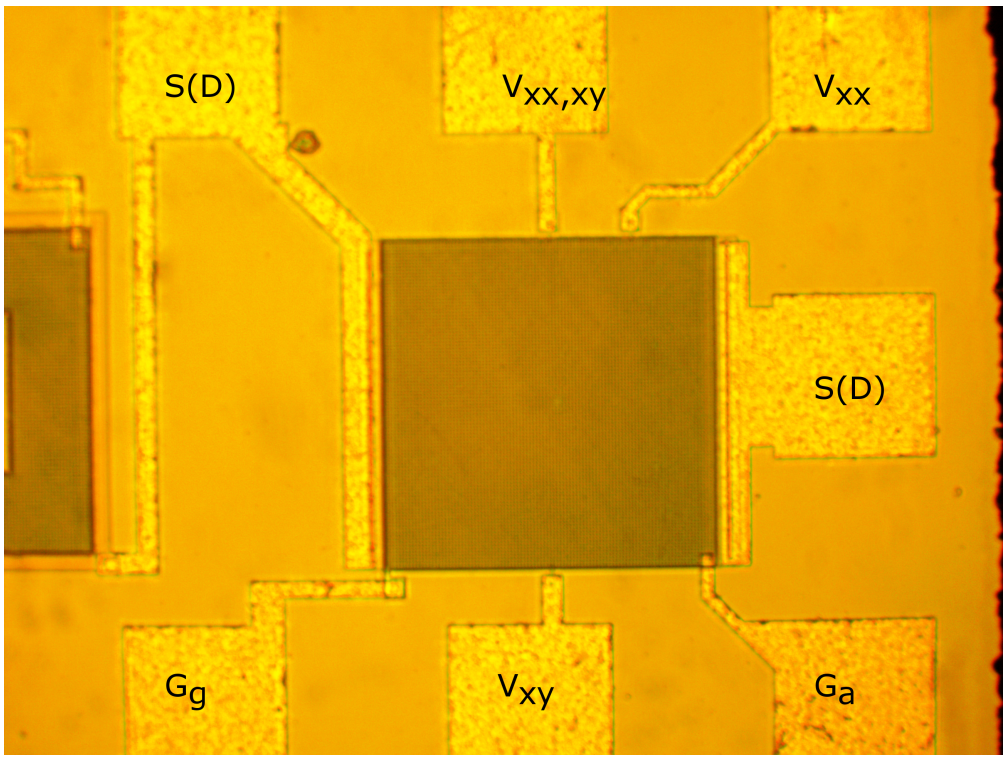

Figure 3.2: Optical image of AA with signed contact pads

must be as small possible as they are assumed to probe the potential value at some particular point of the system. Besides, potential contacts are good conductors (also heavily doped with donors silicon), therefore they can be considered as equipotential. If the contact to the system is relatively big, this contact influences local current distribution that makes data analysis more difficult. For investigated system width/length between potential contacts relation $\frac{w}{l_0} = 4$.

All cryosystems have a stick which has batch of wires for electrical link of connectors on the top and on the bottom of the stick. Top connectors are just connected to macroscopic wires going to different measuring devices as lock-in amplifiers. The bottom part of the stick has a place for holding the sample. But it is also needed to link connectors of the stick and contact pads of the sample. Specific type of plate for substrate depends on the cryostate. For the most part of measurements textolite plate with 8 gold tracks and soldered wires with dip-pins was used (see fig.3.3) as cryostate stick had dip-connectors in the lower part. The substrate was attached to the plate by using BF-2 glue. Connecting of the contact pads from sample and tracks from plate was made either manually using silver paste or with help of manual wire bonder Kulicke and Soffa 4523 AD that basically welds micro wires. Used wires were either golden or 1-% Si/Al alloyed threads with thickness 20-30 microns.

Multiple chips of the same design were fabricated on the same wafer. Probably due to inevitable temperature gradients during the fabrication, AA on different chips demonstrated different low-temperature transport properties such as charge carriers peak mobility or oxide layer thickness. The experiments were carried out on several samples with effective peak mobility of electrons in

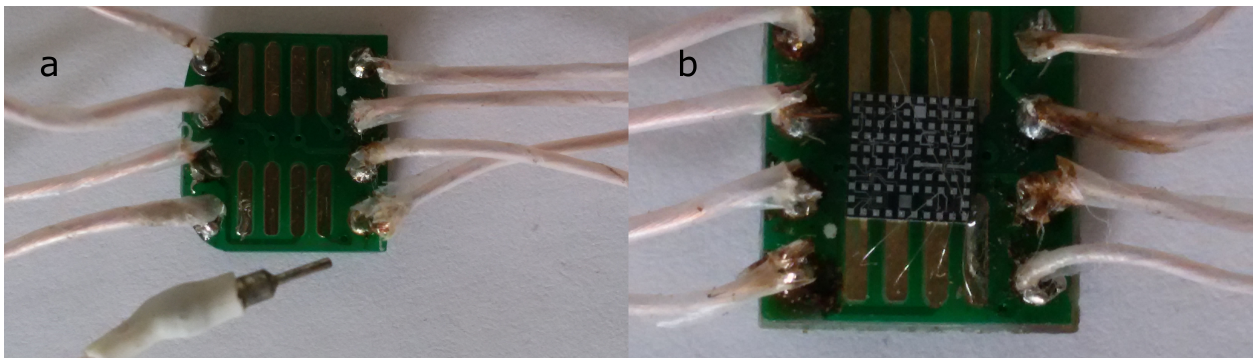

Figure 3.3: (a) Textolite plate with soldered dip-pin wires (b) The same plate with glued substrate and welded wires

AA in wide range from 400 to 5000 cm^2/Vs. Despite this spread of mobilities, most of the observed phenomena were shown up in all samples. The mobility had impact only on the magnitude of the corresponding effects. We demonstrate the data from the representative high mobility sample AA1 and low mobility sample AA2.

3.2 TEM

For detailed sample analysis transmission electron microscope (TEM) FEI Titan 80-300 from National Research Center Kurchatov Institute was used. The pictures were obtained by Prikhod'ko Kirill at the energy of 200keV. The pictures in TEM are produced by transmitted electrons therefore there is a requirement for thickness of the samples observed in TEM - it has to be not larger than 100nm. The cross-section thin lamella for TEM studies was cut out from the surface region (shown

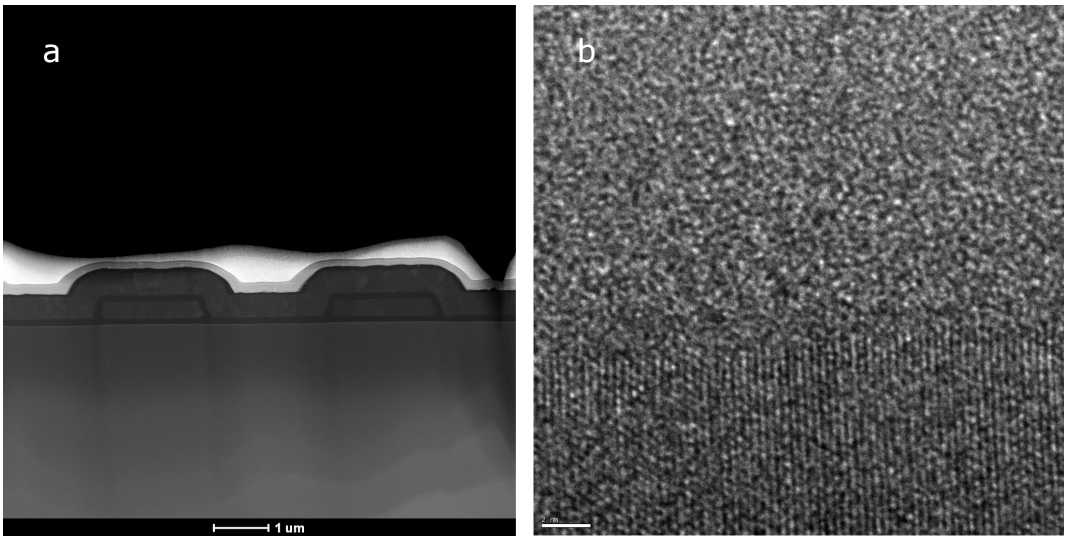

Figure 3.4: Examples of pictures obtained on TEM: (a) in scanning mode (STEM), scale bar is 1μm; (b) in transmission mode the interface of Si/SiO_2. Scale bar is 2nm

by dashed line on fig.3.1b) of the sample using FEI Helios NanoLab 650 focused Ga-ion beam. The pictures were made as in scanning mode (STEM, see fig.3.4a) when the electron beam is focused

in dot that moves across the sample, as in conventional mode (see fig.3.4b) for determination of the smoothness of the transition.

3.3 Magnetotransport measurements

Magnetotransport measurements are one of the main method for investigation of diverse systems. They are based on the ability of the systems to conduct electrical current. The output data from such type of measurements is the dependence of conductivity (resistivity) tensor, i.e. the longitudinal and transverse components, from temperature, magnetic field and other external parameters. As it was shown above, this data is enough to determine the density and mobility of the charge carriers in the system. More complex analysis of SdHO and weak localization, for example, can provide the information about effective mass, mean free path, phase coherence length etc.

Magnetoresistance measurements were performed in the temperature range 0.3-8 K using Cryogenics 21T/0.3K, PPMS-9 9T/1.5K and CFMS 16T/1.8K systems. AC transport current was fixed at value 100nA to avoid overheating. All measurements were carried out in the frequency range 13-18Hz using a standard 4-terminal technique. In 4-terminal technique two contacts are used for current input/output and voltmeter is connected between the rest ones that are connected directly to the system. In order to compensate contact asymmetry, magnetic field was swept from positive to negative values and resistance per square (Hall resistivity) data was then (anti)symmetrized.

As the AC voltage V source internal generator of lock-in amplifier SR-830 (Stanford Research Systems) was used. The resistance of investigated AA has an order of tens of kOhms, therefore the current was set by resistor with resistance R of order of 1 or 10MOhm which was connected with AA in series and hence, the transport current $J = \frac{V}{R}$. For setting gate voltages the sources of DC voltage Keithley 320 Programmable Voltage Source, Yokogawa GS200 and internal source of DC voltage of lock-in were used. As voltmeters the same lock-in amplifiers SR-830 were used. V_{xx} value was obtained from lock-in connected between V_{xx} and V_{xxxy} contact pads, V_{xy} value - from lock-in connected between V_{xxxy} and V_{xy}. Investigated AA has constant width w=0.4mm along the whole sample therefore these expressions are valid:

$$\begin{aligned} j = j_{xx} &= \frac{J}{w} \\ E_{xx} &= \frac{V_{xx}}{l_0} \\ E_{xy} &= \frac{V_{xy}}{w} \end{aligned} \tag{3.1}$$

where l_0=0.1mm is the distance between V_{xx} and V_{xxxy} contacts (where they are connecting to the AA). These equations lead to the following ones:

$$\rho_{xx} = \frac{V_{xx}}{J}\frac{w}{l_0}$$
$$\rho_{xy} = \frac{V_{xy}}{J} \tag{3.2}$$

All measurements were made in the regime of highly conductive media. Indeed, measured resistance per square (that is always elevated with respect to the S2DEG local resistivity due to bottleneck effect) is lower than the resistance quantum $h/e^2 \sim 25.8$ kOhm. Therefore the quasi-classical treatment of the transport is applicable.

3.4 Cryomagnetic system

Cryomagnetic system is just a cryostat with a superconducting magnet inside. Cryostat is just the double-wall flask (Dewar flask). Inside the flask helium-4 ^{4}He liquid is poured. Helium is used as the substance that lets to obtain the lowest temperatures, its boiling point is 4.2K at atmospheric pressure. The design of cryostat is aimed to keep the liquid helium (and, therefore, low temperatures) inside as long as possible. Another important task is the temperature stability inside the cryostat, but these criteria are satisfied simultaneously. Between internal and external walls there is a reservoir for liquid nitrogen (boiling temperature 77.4K for atmospheric pressure) for lowering the temperature of helium reservoir walls that leads to the reduction of the heat transfer of the helium and the room. Also between the walls the vacuum is maintaining as the main temperature transfer is carried out by gas. Internal walls are covered with so-called super-insulation plastic film that has very poor thermal conductivity with some metal coating (aluminum, for example) for reflecting of external radiation. Inside the helium reservoir there are also several reflecting screens for preventing radiation from the top part of cryostat that has room temperature.

The particular structure of cryomagnetic system differs for different systems. Here the internal structure and the principle of work of cryomagnetic system Cryogenics 21T/0.3K are described (see fig.3.5a). The most part of measurements were performed using this system. This facility can provide magnetic fields up to 21T and temperatures down to 0.3K.

The main element of this system that let to get such low temperatures is Variable Temperature Insert (VTI). This is the insert in the cryostat along the central axis that, in fact, is mini-cryostat by itself. The stick with sample on the holder (Probe) is placed inside VTI. In this facility VTI with helium-4 (1.5K is the minimal temperature) and VTI with helium-3 (minimal temperature is 0.3K) can be used. Let's consider the structure of the latter one (fig.3.5b).

Internal walls restrict the volume where Probe is placed. Also, as in conventional cryostat there is a vacuum between internal and external walls for the reduction of the heat transfer between

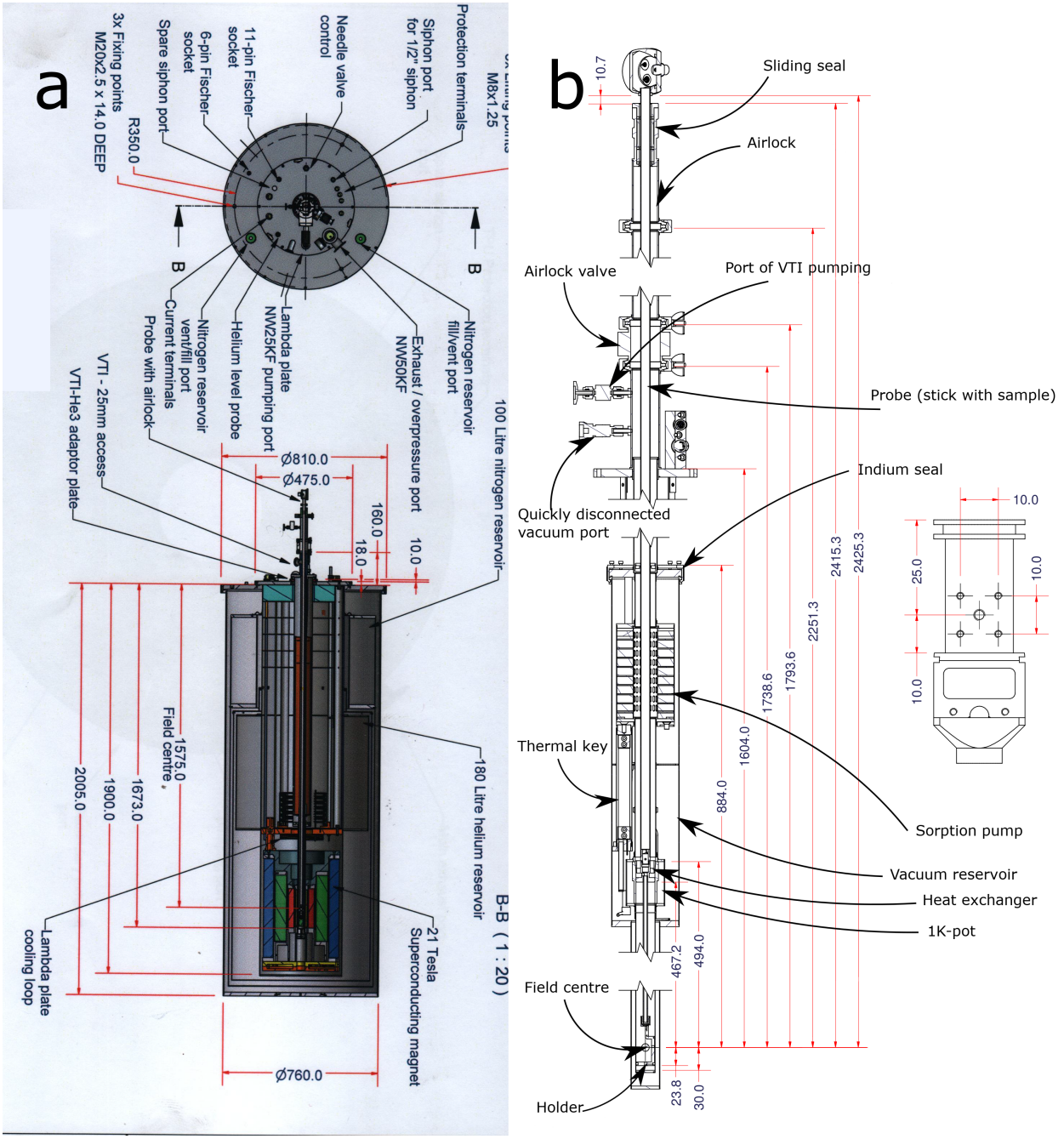

Figure 3.5: (a) The scheme of cryomagnetic system; (b) more detailed scheme of VTI - the most important part of the facility. The sketch of sample holder is shown on the right

VTI and surrounding helium-4 in the main cryostat. Temperature transfer gas in this VTI is helium-3 that is very expensive gas therefore the system consisting of the internal volume of VTI and the external reservoir for helium-3 is sealed for prevention as helium-3 leakage as getting extraneous substances inside. For control of helium-3 concentration in this system sorption pump is used. It is, in fact, the absorbent carbon volume that is placed between internal and external walls of VTI and having holes in the internal volume of VTI. At low temperatures (4-10K) carbon absorbs the gas from the volume, whereas at high temperatures (higher than 30K) it releases absorbed gas to the volume. The temperature of sorption pump rises by using heater and drops by turning on the

heat contact between pump and degree chamber (see below).

The important part of VTI is 1K-pot that is placed between the walls below sorption pump. This is just the chamber that is connected with the helium reservoir of the main cryostat through narrow capillary. Capillary is equipped with needle valve - threaded cone that can move opening or closing the capillary. Unlike the conventional ball valve that has, in fact, only two positions (open and closed) as the step of the valve is macroscopic, needle valve can regulate the flow through the capillary. Also 1K-pot can be connected through the hose either to helium net (the external system of pipes that collects evaporated helium from all facilities of the building for further liquefaction) or to pump pumping to the helium net. The liquid helium in the reservoir of the main cryostat is held under the pressure slightly higher than atmospheric one. Therefore, pumping the 1K-pot the liquid helium from the reservoir of the main cryostat will flow to the 1K-pot. Adjusting this flow by needle valve the dynamic equilibrium can be reached - the arrival of the helium from the capillary will be equal to the amount of helium pumping out of the 1K-pot. Thus, the 1K-pot will be filled with liquid and the saturated steams of helium under pressure lower than the atmospheric one. The pressure of saturated steams is directly related to the temperature and in 1K-pot the temperature down to 1.5-1.8K can be obtained. The temperature of the 1K-pot is called the base temperature. The 1K-pot sets the temperature of the gas inside the VTI at the base temperature value on the height of 1K-pot. For this purpose 1K-pot is connected with the brass-copper element (having good thermal conductivity) another edge of which is the internal wall of the VTI on this level. If the temperature of the sample below the 1K-pot is higher than base temperature, the convection process in the internal heat transfer gas is activated.

The sample is placed on the holder of the Probe, i.e. almost on the bottom of the VTI. The set of temperature of the sample depends if this temperature is higher of lower than base temperature. If the desired temperature is higher than the sample is just heated up by the heater on the Probe. In this case such temperature of sorption pump is set that there is helium-3 inside the VTI but not very much to prevent very intensive heat exchange. The power of the heater use regulate the temperature of the sample as dynamical equilibrium is set between heater and convection of the gas inside VTI with constant base temperature above the sample. If the desired temperature is lower than the base one, firstly, the sorption pump is heated up to release all absorbed helium-3. The base temperature inside is constant whereas the pressure of helium-3 rises that leads to the condensation of the helium-3 (boiling point is 3.19K for atmospheric pressure). Waiting for some time (from 10 to 40 minutes - it depends on the time which is planned to work with temperatures below base one) for helium-3 condensation, further the temperature is regulated by the temperature of sorption pump. Indeed, inside VTI there are the liquid and saturated steams of helium-3, therefore, as was described above for helium-4 on 1K-pot, the temperature can be regulated by pressure regulation, i.e. absorption/desorption of helium-3 from the volume/sorption pump. Such process can set the

temperatures down to limit 0.3K on the sample.

As it is cryomagnetic system, there should be the sources of magnetic field. In this cryostat for the creation of magnetic field the system of concentric coils is used (see fig.3.5a): three internal ones from Nb_3Sn mounted on the holders from stainless steel, and the external one from $NbTi$ mounted on the aluminum holder. Coils are connected in series on the top dielectric flange. From the most internal and external coils HTSC (high-temperature superconducting) current leads are going up till the level of nitrogen reservoir (while they are still superconducting) for reduction of thermal supply. Then conventional wires are going to the top of the cryosat and connected to the terminals that connects directly to the current source. In parallel with magnet superconducting key is connected. It is used for field fixation. When the field is changing, the heater is working and the key is in normal state, i.e. has non-zero resistance, therefore the current predominantly is flowing through the magnets that are superconducting. If the freezing of the field is necessary the heater is turning off, the key is going to superconducting state, the current through the source is lowering to 0 and the current is closed in circuit key-magnet. At T=4.2K coils can produce maximum 20T. There is a lambda-plate above the magnet which, in fact, is the same as 1K-pot, i.e. the cavity that can be pumped and is connected with helium reservoir through the capillary regulated by needle valve. The principle of the temperature decrease is the same as was described above for 1K-pot. The thermal conductivity of liquid helium is very low, so that the cooling of the helium above the plate does not occur, but below the plate the convection is activated: the helium is at 4.2K, the plate has lower temperature. This way the temperature of the magnet can be lowered down to 2.5K. Critical current at this temperature is higher and the maximum field obtained in this facility is 20.939T.

Chapter 4

Results

4.1 Effective density

Investigated system is heterogeneous therefore it is considered as effective media. It is straightforwardly characterized by effective Hall density ($n_{eff} \equiv [eR_{xy}(B = 1\mathrm{T})]^{-1}$ from expr.2.26) and effective carrier mobility ($\mu_{eff} \equiv (n_{eff} e \varrho)^{-1}$ also from expr.2.26). Here and further ϱ is the measured resistance per square.

Firstly, the n_{eff} dependency on V_g and V_a was analyzed. Experimentally observed $n_{eff}(V_g)$ dependencies (for three various V_a values, shown on fig.4.1) are in contrast with the expectation of linear dependency for homogeneous system. The reason for the deviations is artificial non-uniformity of the system. Such behavior reflects different regimes of transport current flow distribution. It is possible to distinguish the ranges of gate voltages that correspond to various current density distribution (schematically shown by letters (a)-(d) in the main panel and also in the corresponding panels under the graph on fig.4.1). The higher transport current density is shown by lighter color.

For V_g high enough (figures 4.1(a) and 4.1(b)), S2DG is very conductive because of high electron density. Due to edge effects and larger gate-to-2DEG distance, shells have lower electron density and hence smaller conductance. Therefore, transport current flows predominantly through the S2DG and Hall effect, i.e. $n_{eff}(V_g)$, is determined by its density. It means that the islands have small impact on $n_{eff}(V_g)$ dependence.

For small values of V_g (figures 4.1(c) and 4.1(d)) the S2DG density and conductivity decreases and contribution of islands to the transport rises. Increase of the V_a value makes the islands much more conductive than S2DG. Therefore transport current prefers to flow through islands and minimizes the path through the S2DG. Thus the effective density n_{eff} increases (relatively to density defined by V_g) since the Hall voltage is determined by the islands. As V_g increases, the contribution of depleted S2DG rises leading to the drop of the n_{eff} (figure 4.1(d)).

For V_g and V_a low enough, both S2DG (unlike case **b**) and islands (unlike case **d**) are poorly conductive. Low conductance of both regions force transport current to flow through the whole perimeter of the shell. This leads to the elevated role of the low-density shells and the visible

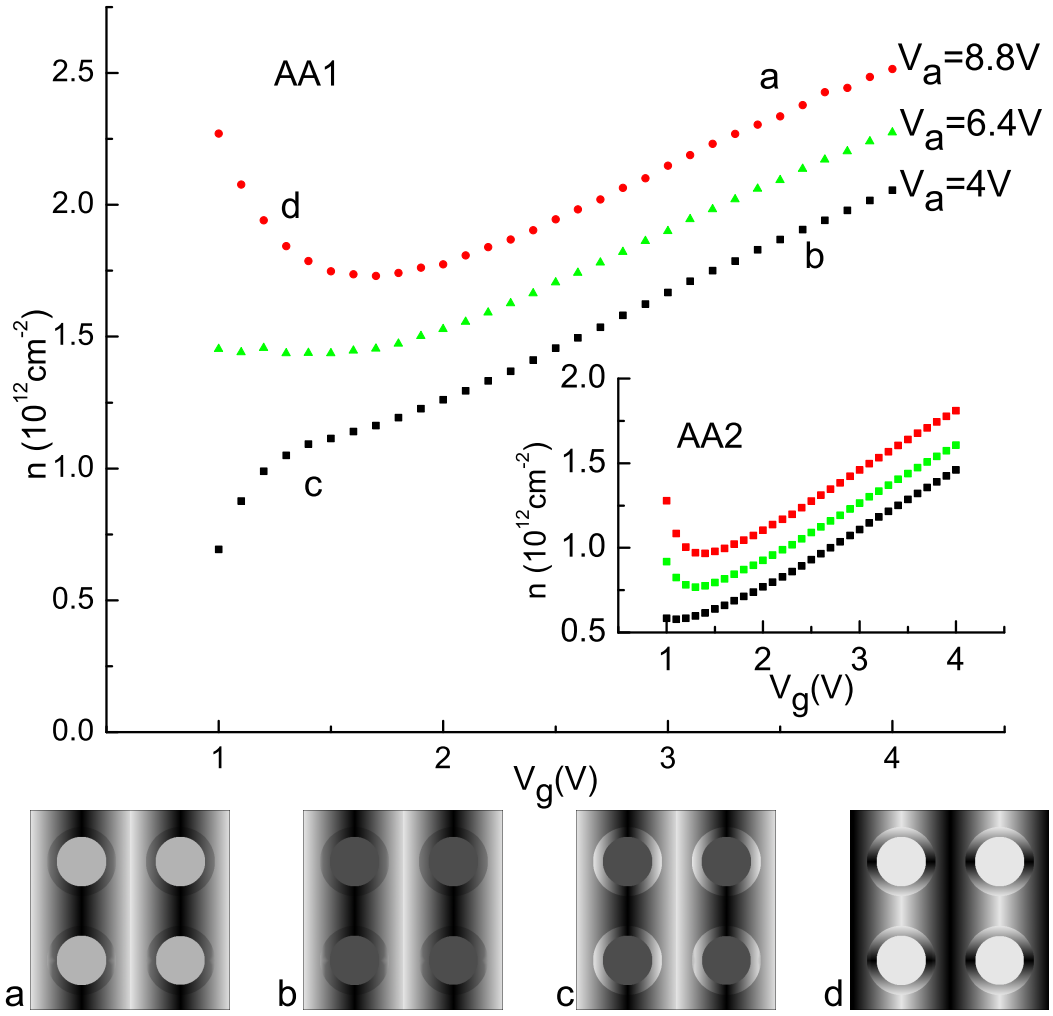

Figure 4.1: The Hall density at T=1.8K for sample AA2 vs S2DG gate voltage for three representative island gate voltages. Inset shows the similar data for the high-mobility sample AA1. In panels (a)-(d) the higher electron density the lighter area. Panels (a)-(d) correspond to the domains of the voltages designated by the same letter on the graph.

increase of the Hall voltage, i.e. drop of n_{eff} value (case **c** on the fig.4.1).

The effective density data, shown in fig.4.1, demonstrating an enhanced drop in low-V_a/ low-V_g region, were obtained for low-mobility sample AA2. For high-mobility sample AA1 (inset to fig.4.1), despite the absence of the drop, a similar tendency is clearly seen: n_{eff} value decreases with V_g growth at high V_a and this effect vanishes as V_a is lowered. This data show that the effective density in the macroscopically inhomogenious systems follows the same physics irrespectively of mobility.

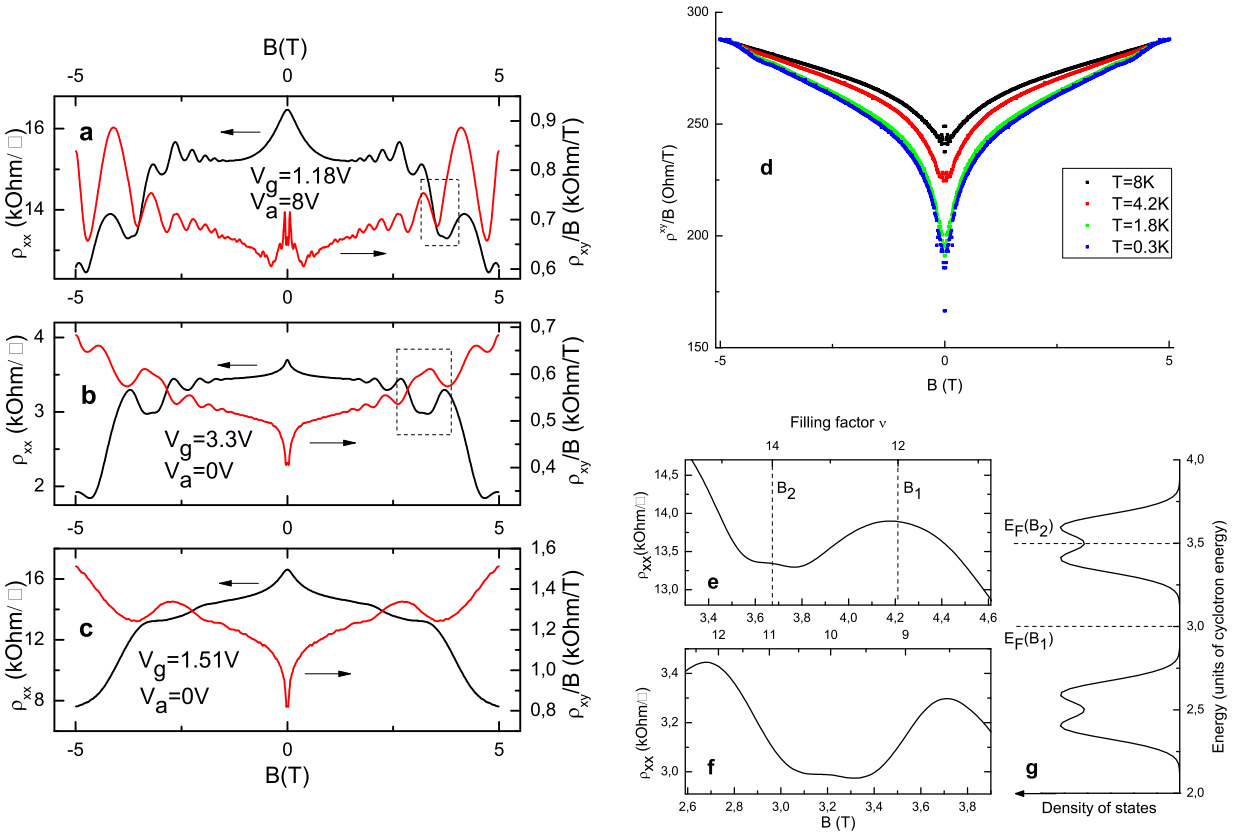

Figure 4.2: Magnetoresistance (black curves) and Hall coefficient (red curves) of sample AA1 at T=0.3K in regime of current through antidots (a), current through S2DG (b) and elevated role of shells (c). (d) Hall coefficient of sample AA2 vs magnetic field for four different temperatures. For convenience, curves shifted such that their edges (at B=5T) coincide (curve for 0.3K remained unchanged). (e) and (f) are enlarged areas from panels (a) and (b), respectively, shown by dashed rectangles which demonstrate the splitting of minima of magnetoresistance. (g) Schematics of Zeeman-splitted Landau levels in density of states vs energy diagram. Fermi levels for magnetic fields B_1 and B_2 (indicated in panel (e)) are shown by dashed lines.

4.2 Magnetoresistance and Hall measurements

Thus, different regimes of current transport in artificially inhomogeneous tunable media were established. In order to explore the differences between the regimes **b**, **c**, and **d** (here and further designations are taken from fig.4.1) more detailed magnetotransport measurements were performed. We chose Hall coefficient (R_{xy}/B) to visualize the difference between AA and uniform system, where R_{xy}/B is roughly field-independent.

Fig.4.2(a) shows magnetoresistance (ϱ) and Hall coefficient in the regime **d** where transport is dominated by islands. Though the effective ϱ is about 15 kOhms (i.e. $\sim e^2/h$), pronounced SdHO are observed due to the high mobility electron gas in the islands. Electron density obtained from SdHO ($n_{SdH} \approx 1.4 \times 10^{12}\text{cm}^{-2}$) is higher than the Hall density ($n_{eff} \approx 1 \times 10^{12}\text{cm}^{-2}$) because the latter is affected also by S2DG bottlenecks. Hall coefficient is a non-monotonic function of magnetic field with a *maximum* at $B = 0$.

For comparison in fig.4.2(b) magnetoresistance and Hall coefficient of the system in regime **b** with $V_a = 0$ are shown. V_g value was adjusted to make n_{eff} approximately equal to the value from fig.4.2(a). Effective $\varrho \approx 3$kOhms value is about 5 times less because S2DG in this case is well-conductive and transport current bypasses the depleted regions. SdHO are also observed with $n_{SdH} \approx 0.9 \times 10^{12}$cm^{-2} comparable to $n_{eff} \approx 1.2 \times 10^{12}$cm^{-2}. At $B = 0$ Hall coefficient in this case has *minimum*.

Finally, fig.4.2(c) shows magnetoresistance and Hall coefficient in low-density regime somewhere between **b** and **c**. The gate voltages were adjusted to make ϱ approximately equal to the value from fig.4.2(a). The behavior of the transport is completely different from fig.4.2(a) and qualitatively similar to fig.4.2(b) without SdHO. Hall coefficient has *minimum* at zero field. This data straightforwardly demonstrates that contrary to non-modulated 2DES, the magnetotransport reflects complexity of carrier density redistribution and is not determined by the value of the effective resistivity.

The common tendency for all Hall coefficient data is the growth with the magnetic field. In homogeneous system Hall coefficient is constant and directly corresponds to electron density $R_{xy}/B = 1/ne$. In the studied system there are regions with different densities. For Si MOSFETs it is known that electron mobility is density-dependent (μ generally grows with n, then reaches a steep maximum and decreases slowly for very large carrier densities) [38]. In magnetic field the longitudinal conductivity σ_{xx} decreases $\propto (1+(\mu B)^2)^{-1}$, i.e. the higher the mobility, the faster the decrease. Thus, with increasing the field the conductivity of low-density regions decreases slower than the one of high-density regions. Since the current prefers to flow through high-conductive regions, with increasing field current redistributes so that the role of low-density low-mobility regions increases. Therefore, Hall coefficient should rise, in agreement with experimental data. Exactly this mechanism was suggested in the paper[39] with first measurements of these samples.

In small magnetic field Hall coefficient experiences an abrupt feature. The bare 2D gas in Si-MOSFETs also has a small low-field Hall nonlinearity, discussed in detail in Ref.[40] and reported for the similar samples in Ref.[39]. However, the huge amplitude of the low-field Hall coefficient variation in fig.4.2 clearly identifies it with the sample nonuniformity. Interestingly, low-field quenching of transverse magnetoresistance (and even change of its sign) has already been explored in various artificially inhomogeneous and mesoscopic systems. First experiments in 1D wires by Roukes [41] were further theoretically explained [42] by scrambling of electron trajectories on crossroad in a place of contacts. The authors speculated that quenching is unambiguous manifestation of 1D transport. Here it is worth to note that all available theories in 1D or 2D systems are essentially ballistic. In further experiments with ballistic antidot arrays[43] the quenching of the Hall effect was also observed, although the qualitative pinball picture didn't account for attenuation of Hall coefficient. In the more recent experiments on 2D systems with AA [44] the observed

quenching of Hall effect was confirmed by numerical simulations, but no physical mechanism was suggested.

Investigated here system is essentially different, because the transport is diffusive and the inhomogeneities are tunable from dots (areas of low potential, $V_a > V_g$) to antidots (areas of high potential, $V_a < V_g$). Zero-field Hall coefficient in our experiments can either grow or fall with B depending on V_g and V_a. Origin of different behavior is unclear and requires further theoretical investigation. Suppression of the zero-field Hall coefficient quenching with temperature (fig.4.2(d) for sample AA2) is the indicator, that this feature is related to weak-localization phenomenon. We believe that low-field feature in Hall coefficient comes from redistribution of transport current in the regime of weak localization. This assumption is totally nontrivial: firstly, it is a textbook knowledge that in homogenous medium weak localization does not influence the Hall resistivity[45] and, secondly, the relative value of the observed nonlinearity is rather high (few 10%), larger than weak localization correction to resistivity in the bare 2D gas. Present results thus call for theoretical modeling of the weak localization in the presence of macroscopic modulation. Moreover, it might be that sample inhomogeneity is a clue to understanding the often observed and not always explained low-field feature in the other 2D systems [40, 46, 47].

Another unusual, yet high-field magnetotransport effect is the splitting of the minima of the longitudinal magnetoresistance ϱ (enlarged domains from figs.4.2(a-b) are shown in figs.4.2(e-f)). As a rule, as magnetic field increases, and Zeeman term exceeds the temperature and Landau level broadening (see fig.4.2g for the schematics of the density of states), the resistivity maxima are split. Indeed, in uniform 2D systems in SdH domain Hall resistivity ρ_{xy} is higher than ρ_{xx} and the maxima of the conductivity $\sigma_{xx} = \rho_{xx}/(\rho_{xx}^2 + \rho_{xy}^2) \approx \rho_{xx}/\rho_{xy}^2$ at the half-integer filling factors correspond to the maxima of the resistivity and maxima of the density of states.

In samples that investigated here, effective resistance per square ϱ is higher than R_{xy} in SdH domain. If the areas of antidots were just infinite barriers for electrons, it would only change the geometrical factor w/l and would not turn minima to maxima. In other words, the resistance per square should increase but the $\varrho(B)/\varrho(B=0)$ ratio should remain unchanged. Meanwhile in our system ϱ_{xx} *minima* appear to be splitted. It is worth to note that splitting is observed both in regime **b** (current through S2DG) either in regime **d** (current mainly through islands).

We suggest that this splitting might be explained if the equation $\sigma_{xx}^{eff} = \varrho/(\varrho^2 + R_{xy}^2)$ holds correct for the resistance per square. Then $\sigma_{xx}^{eff} \approx 1/\varrho$ and conductivity maxima (coinciding with the maxima of Zeeman-splitted density of states at Fermi level, shown in fig.4.2g) correspond to the resistance per square minima. This suggestion is not expected to be valid because conductivity and resistivity are local properties, whereas the resistance per square is the macroscopic characteristic of the sample. In other words, effective conductivity approach is surprisingly applicable not locally but rather to the overall system.

4.3 Metallic behavior of resistivity

Since in some of models suggested for explanation of metal-insulator transition in 2D systems the system was believed to be essentially non-uniform at the microscale [48, 50, 49] it was decided to examine how the artificially tunable inhomogeneity in presented here AA affect 2D "metallicity".

In order to quantify "metallicity" experimentally it was taken the relative variation $\kappa \equiv (\varrho_{7.4} - \varrho_{1.8})/\varrho_{1.8}$, where $\varrho_{1.8}$ and $\varrho_{7.4}$ values were measured at experimentally convenient temperatures 1.8K and 7.4K respectively. Thus, κ never drops below -1, and relatively big positive values of κ correspond to strong "metallic" behavior and negative values - to insulator. Figure 4.3(a) shows κ versus V_g dependence for different values of V_a for high-mobility sample AA1. The inset shows a similar series of $\kappa(V_g)$ dependencies for low-mobility sample AA2. Insignificant distinction is that temperature reference points used for sample AA2 were 2.1K and 8K, respectively. This difference is connected only with experimental conveniences.

At high values of V_g, when the system is deep in the conductive domain κ tends to zero for both low and high-mobility samples. This behavior is caused by (i) weakening of electron-electron interactions at elevated densities and (ii) domination of the S2DG in conductance of the system, i.e. transport properties of antidot array for large V_g are equivalent to bare 2D gas, as expected.

For small values of V_g κ depends dramatically on the value of V_a and on the mobility of the sample.

For high-mobility sample and small values of V_a there is a strong "metallic" conductivity: κ is positive, quite large (about 1.5), and drops monotonically with V_g, as it should be for bare 2D gas in Si-MOSFET[35], because the islands areas are out of the game. However for high values of V_a "metallic" conductivity becomes suppressed for all values of V_g and κ for sample AA1 becomes

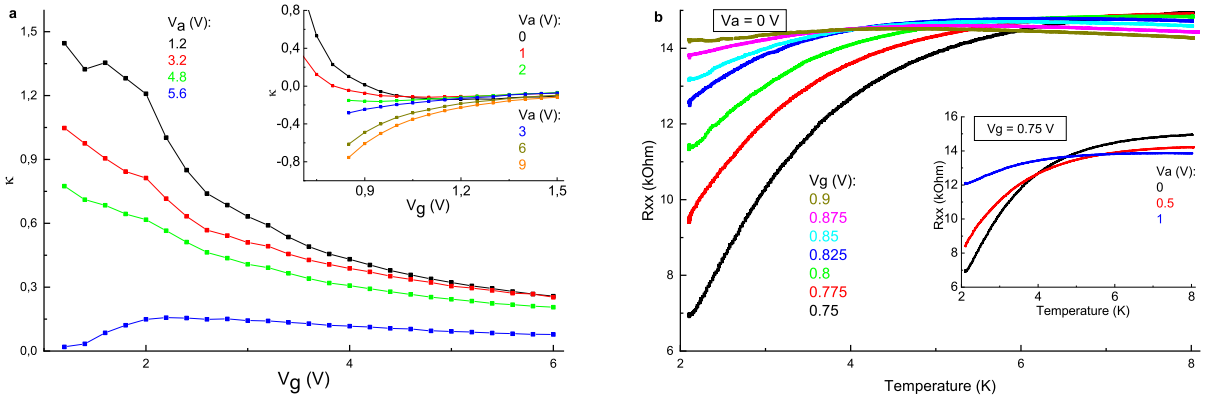

Figure 4.3: (a) Relative change of resistivity of AA1 with temperature (from 1.8K to 7.4K) κ vs S2DG voltage for different voltage on antidots gate. The same data (but for temperatures 2.1K and 8K) for low-mobility sample AA2 is shown on inset. (b) Temperature dependence of resistivity of the sample AA2 at fixed V_a=0V for different V_g. The same data at fixed V_g for different V_a is shown on inset.

non-monotonic and goes to zero at small V_g.

For low mobility sample AA2 as V_a increases weakly positive κ for low V_g turns to negative. Fig.4.3(b) represents the temperature dependence of the resistivity of low-mobility sample. On the main graph dependencies for different S2DG voltage V_g and same antidots voltage V_a are shown to demonstrate the degeneracy of metallic behavior with increase of V_g. The same tendency with V_a increase at fixed V_g is reflected in inset. In other words filling the islands with electrons turns the system to "insulating" behavior, no matter how large the mobility is.

The following explanation of this phenomena is suggested. For small values of V_a islands areas are "closed" for electrons. However for high values of V_a current flows to the islands and, as result, inevitably flows through the shells. The latter have strong insulating behavior that cause the suppression of κ. Thus, we demonstrate and explain qualitatively that our effective media allows to tune 2D "metallicity".

This observation might also help to understand the answer to the question why the strength of the metallicity in Si-MOSFETs is the highest among other system despite the relatively low mobility. Indeed, in the highest mobility Si-MOSFETS ($\mu_{peak} \sim 3 - 4 \cdot 10^4 \text{cm}^2/\text{Vs}$), the resistance increases almost by an order of magnitude with temperature[35], and strong metallicity is observed at relatively high carrier densities (few 10^{11} cm^{-2}). In the other material systems with mobilities exceeding 10^5 cm^2/Vs and much lower carrier densities ($\sim 10^{10}$ cm^{-2}, e.g. Si/SiGe quantum wells[51], n-GaAs [52], p-GaAsTO[53], etc.) the growth of the resistivity with temperature is typically smaller than a factor of 2. All these high mobility systems have smooth impurity potential, similarly to tunable part of potential due to artificital modulation in the antidot array. This potential might be one possible mechanism for the metallicity suppression. Indeed, in low carrier density materials the relative fluctuations of charge distribution are much larger and their role should be re-examined.

Chapter 5

Discussion

5.1 Metal-insulator transition point

Since Ioffe and Regel[54] it is common knowledge that the boundary between metal and insulator corresponds to $k_F l \sim 1$. In uniform 2D systems this criterion means that the conductivity is about $e^2/h \sim 1/26$ kOhm . Below this value the wave functions at Fermi energy are localized and system is supposed to have insulating temperature dependence of the resistivity. Above this value the temperature dependence of the resistivity within non-interacting picture should be either weak insulating or metallic, in case of strong electron-electron interactions. The ultimate boundary between metal and insulator can be, of course, introduced only at $T = 0$, when the coherence length is infinite. For macroscopic antidot array similar to investigated here, the low temperature limit can hardly be achieved, since it requires mK and sub-mK temperatures. S2DG is responsible for metal to insulator transition, while the geometrical factor (effective length-to-width ratio) in such system is enhanced. Therefore the threshold resistance per square in antidot array is elevated, and 26 kOhm is not a dogma for macroscopically modulated system anymore. E.g. in presented here samples vanishing temperature dependence of the resistivity for about 50-80 kOhm effective sample resistance was observed.

5.2 Phase diagram.

The results are summarized in the phase diagram of the system in $(V_g; V_a)$ plane in fig.5.1. For very low values of V_g the system doesn't conduct, i.e. it is in insulating state. For low values of V_g the value of V_a is decisive. If V_a is high enough, the system is in the island-dominated regime: current flows in the low-resistance islands and minimizes the path through the narrow bottlenecks between them. In this regime Hall density is elevated and Shubnikov-de Haas density is given by islands. Metallic temperature dependence of the conductivity is suppressed because total resistivity of the system is determined by bottlenecks between islands and S2DG.

For low values of V_a the system is in the "shell-dominated" regime when current flows without preferences spreading out over the whole system. And for high values of V_g again there is

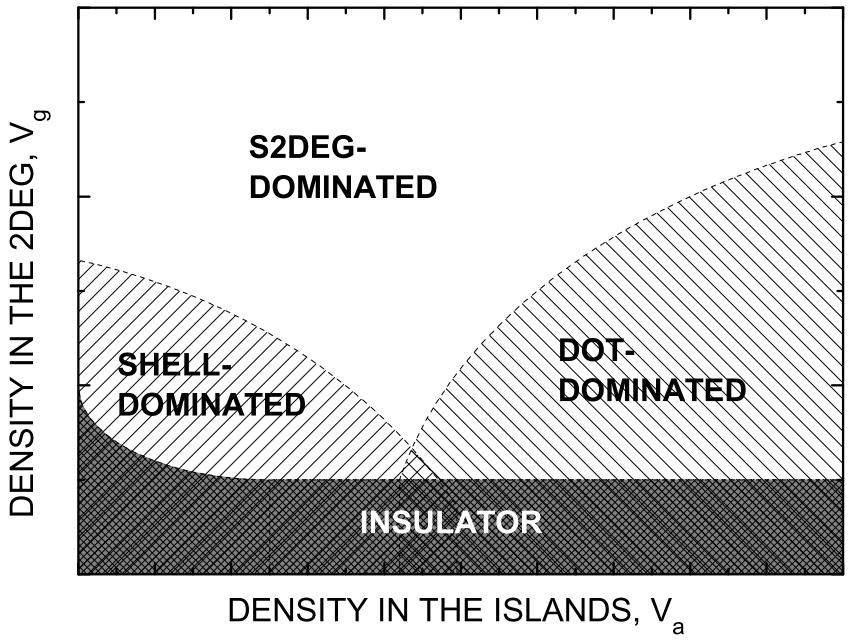

Figure 5.1: Schematic phase diagram of the system in space of S2DG (vertical) and islands (horizontal) electron density.

no big difference between low and high values of V_a because islands are almost out of the game, the system is in the S2DG-dominated regime: current bypasses islands flowing through S2DG.

Role of periodicity. Interestingly, the periodic structure (i.e. equivalence of all islands and inter-island necks) is important. In our case the period of the structure is 5 μm and there are only 80 periods across the 400 μm wide sample. If the system was more random, like e.g. [55], transport through it would be governed by percolation cluster and lateral cluster size could easily exceed 80 periods. In this case the properties of the system would be irreproducible and very large samples were needed for averaging, thus hindering the systematic studies and possible applications.

Chapter 6

Conclusion

To sum up, transport properties of the macroscopically non-uniform and tunable Si-based 2DES were experimentally examined. Such system has two gates for controlling the densities in the islands and residual 2D gas separately. The conductive properties of this system turn out to depend on both gate voltages V_g and V_a. In order to explain different behavior of the system under different gate voltages simple classical considerations about the current flow within 2DES were applied. The phase diagram of the system in coordinates electron density in the islands vs electron density in the 2D gas was defined. In this phase diagram various transport regimes were identified from the analysis of the Hall effect and magnetotransport: insulating, 2D gas dominating, island dominating and shell dominating.

In high magnetic field, independently on the regime of transport, Hall coefficient grows with field, in agreement with current flow redistribution towards the lower density lower mobility regions[39]. The behavior of the Hall coefficient in low magnetic field is puzzling. The sign of the low magnetic field correction to Hall effect depends on whether conductivities of the islands are high or not. Temperature and magnetic field dependencies of the low-field Hall effect were explored, it turned out that they are quite strong that signifies that this low-field feature is presumably related to weak localization. This observation is not trivial and yet has to be explained. At elevated magnetic field, in the domain of Shubnikov-de Haas oscillations a novel effect was uncovered - Zeeman splitting of the resistivity minima, opposite to Zeeman splitting of the resistivity maxima, observed in homogeneous systems. Also the suppression of the metallic temperature dependence of the resistivity, inherent for Si-MOSFETs, was demonstrated and qualitative explanation of this effect was proposed.

Bibliography

[1] K.S.Novoselov, A.K.Geim, S.V.Morozov, D.Jiang, Y.Zhang, S.V.Dubonos, I.V.Grigorieva and A.A.Firsov, Science **306**, 666 (2004)

[2] M.Chhowalla, H.S.Shin, G.Eda, L.J.Li, K.P.Loh and H.Zhang, Nature Chemistry **5**, 263 (2013)

[3] X.-L.Qi and S.-C.Zhan, Rev. Mod. Phys. **83**, 1057 (2011)

[4] K.S.Novoselov, A.Mishchenko, A.Carvalho and A.H.Castro Neto, Science **353**, 9439 (2016)

[5] Z.Han, A.Allain, H.Arjmandi-Tash, K.Tikhonov, M.Feigel'Man, B.Sacépé and V.Bouchiat, Nature Physics **10**, 380 (2014)

[6] Y.Cao, V.Fatemi, A.Demir, S.Fang, S.L.Tomarken, J.Y.Luo, J.D.Sanchez-Yamagishi, K.Watanabe, T.Taniguchi, E.Kaxiras, R.C.Ashoori and P.Jarillo-Herrero, Nature **556**, 80 (2018)

[7] Y.Cao, V.Fatemi, S.Fang, K.Watanabe, T.Taniguchi, E.Kaxiras and P.Jarillo-Herrero, Nature **556**, 43 (2018)

[8] C.R.Dean, L.Wang, P.Maher, C.Forsythe, F.Ghahari, Y.Gao, J.Katoch, M.Ishigami, P.Moon, M.Koshino, T.Taniguchi, K.Watanabe, K.L.Shepard, J.Hone and P.Kim , Nature **497**, 598 (2013)

[9] D.Weiss, K.Richter, A.Menschig, R.Bergmann, H.Schweizer, K.von Klitzing and G.Weimann, Phys. Rev. Lett. **70**, 4118 (1993)

[10] M.Kuwata-Gonokami, N.Saito, Y.Ino, M.Kauranen, K.Jefimovs, T.Vallius, J.Turunen and Y.Svirko, Phys. Rev. Lett. **95**, 227401 (2005)

[11] B.Abeles, Ping Sheng, M.D.Coutts and Y.Arie, Adv. Phys. **24**, 407 (1975)

[12] D.Weiss, M.L.Roukes, A.Menschig, P.Grambow, K.von Klitzing and G.Weimann, Phys. Rev. Lett. **66**, 2790 (1991)

[13] D.Weiss, K.Richter, A.Menschig, R.Bergmann, H.Schweizer, K.von Klitzing and G.Weimann, Phys. Rev. Lett. **70**, 4118 (1993)

[14] K.Tsukagoshi, S.Wakayama, K.Oto, S.Takaoka, K.Murase and K.Gamo, Phys. Rev. B **52**, 8344, (1995)

[15] D.A.Kozlov, Z.D.Kvon and A.E.Plotnikov, JETP Lett. **89**, 80 (2008)

[16] H.Maier, J.Ziegler, R.Fischer, D.Kozlov, Z.D.Kvon, N.Mikhailov, S.A.Dvoretsky and D.Weiss, Nature Communications **8**, 2023 (2017)

[17] Y.Aharonov and D.Bohm, Phys. Rev. **115**, 485 (1959)

[18] B.L.Alshuler, A.G.Aharonov and B.Z.Spivak, Pis'ma v JETP **33**, 101 (1981)

[19] F.Nihey, S.W.Hwang and K.Nakamura, Phys. Rev. B **51**, 4649 (1995)

[20] Y.Iye, M.Ueki, A.Endo and S.Katsumoto, Jour. Phys. Soc. Jpn. **73**, 3370 (2004)

[21] R.Yagi, M.Shimomura, F.Tahara, H.Kobara and S.Fukada, Jour. Phys. Soc. Jpn. **81**, 063707 (2012)

[22] A.Dorn, T.Ihn, K.Ensslin, W.Wegscheider and M.Bichler, Phys. Rev. B **70**, 205306 (2004)

[23] G.M.Minkov, A.A.Sherstobitov, A.V.Germanenko and O.E.Rut, Phys. Rev. B **78**, 195319 (2008)

[24] S.Goswami, M.A.Aamir, C.Siegert, M.Pepper, I.Farrer, D.A.Ritchie and A.Ghosh, Phys. Rev. B **85**, 075427 (2012)

[25] N.E.Staley, N.Ray, M.A.Kastner, M.P.Hanson and A.C.Gossard, Phys. Rev. B **90**, 195443 (2014)

[26] V.A.Tkachenko, O.A.Tkachenko, G.M.Minkov and A.A.Sherstobitov, JETP Letters **104**, 473-478, (2016)

[27] A.A.Abrikosov Fundamentals of the theory of metals, Moscow "Fizmatlib", 2 edition, chapter 1 (2010)

[28] S.M.Sze Physics of Semiconductor Devices. Book 1, Moscow "Mir", tran., 2 edition, 377 (1984)

[29] S.N.Burmistrov Physical kinetics problems, Dolgoprudniy: Publishing House "Intellect", 62 (2016)

[30] L.D.Landau and E.M.Lifshitz Theoretical physics. Book III. Quantum mechanics (nonrelativistic theory), Moscow: “Nauka”, 4 edition, 532 (1989)

[31] E.Abrahams, S.V.Kravchenko and M.P.Sarachik, Rev. Mod. Phys. **73**, 251 (2001)

[32] E.Abrahams, P.W.Anderson, D.C.Licciardello and T.V.Ramakrishnan, Phys. Rev. Lett. **42**, 673 (1979)

[33] B.L.Altshuler, A.G.Aronov and P.A.Lee, Phys. Rev. Lett. **44**, 1288 (1980)

[34] B.Tanatar and D.M.Ceperley, Phys. Rev. B **39**, 5005 (1989)

[35] S.V.Kravchenko, G.V.Kravchenko, J.E.Furneaux, V.M.Pudalov and M.D’Iorio, Phys. Rev. B **50**, 8039 (1994)

[36] P.T.Coleridge, R.L.Williams, Y.Feng and P.Zawadzki, Phys. Rev. B **56**, R12764 (1997)

[37] Y.Hanein, U.Meirav, D.Shahar, C.C.Li, D.C.Tsui and Hadas Shtrikman, Phys. Rev. Lett. **80**, 1288 (1998)

[38] T.Ando, A.B.Fowler and F.Stern, Rev. Mod. Phys. **54**, 437 (1982)

[39] A.Yu.Kuntsevich, A.V.Shupletsov and M.S.Nunuparov, Phys. Rev B **93**, 205407 (2016)

[40] A.Yu.Kuntsevich, L.A.Morgun and V.M.Pudalov, Phys. Rev. B **87**, 205406 (2013)

[41] M.L.Roukes, A.Scherer, S.J.Allen,Jr., H.G.Craighead, R.M.Ruthen, E.D.Beebe and J.P.Harbison, Phys. Rev. Lett. **59**, 3011 (1987)

[42] C.W.J.Beenakker and H.van Houten, Phys. Rev. Lett. **63**, 1857 (1989)

[43] D.Weiss, M.L.Roukes, A.Menschig, P.Grambow, K.von Klitzing and G.Weimann, Phys. Rev. Lett. **66**, 2790 (1991)

[44] S.de Haan, A.Lorke, R.Hennig, M.Suhrke, W.Wegscheider and M.Bichler, Phys. Rev. B **60**, 8845 (1999)

[45] B.L.Altshuler, A.G.Aronov, in Electron-electron Interactions in disordered systems, edited by A.L.Efros and M.Pollak, Elsevier, Amsterdam (1985)

[46] E. Tousson and Z. Ovadyahu, Phys. Rev. B **38**, 12290 (1988)

[47] G.M.Minkov, A.V. Germanenko, O.E. Rut, A.A. Sherstobitov and B.N. Zvonkov, Phys. Rev. B **82**, 035306 (2010)

[48] B.Spivak, Phys. Rev. B **64**, 085317 (2001)

[49] Y.Meir, Phys. Rev. Lett. **83**, 3506 (1999); Phys. Rev. B **61**, 16470 (2000).

[50] L.A.Morgun, A.Yu.Kuntsevich and V.M.Pudalov, Phys. Rev. B **93**, 235145, (2016)

[51] M.Yu.Melnikov, A.A.Shashkin, V.T.Dolgopolov, S.-H.Huang, C.W.Liu and S.V.Kravchenko, Scientific Reports **7**, 14539 (2017)

[52] M.P.Lilly, J.L.Reno, J.A.Simmons, I.B.Spielman, J.P.Eisenstein, L.N.Pfeiffer, K.W.West, E.H.Hwang and S.Das Sarma, Phys. Rev. Lett. **90**, 056806 (2003)

[53] Y.Y.Proskuryakov, A.K.Savchenko, S.S.Safonov, M.Pepper, M.Y.Simmons and D.A.Ritchie, Phys. Rev. Lett. **89**, 076406 (2002)

[54] A.F.Ioffe and A.R.Regel, Prog. Semicond. **4**, 237 (1960)

[55] G.M.Minkov, A.A.Sherstobitov, A.V.Germanenko and O.E.Rut, Phys. Rev. B **78**, 195319 (2008)